Research Square

Preprints are preliminary reports that have not undergone peer review.
They should not be considered conclusive, used to inform clinical practice,
or referenced by the media as validated information.

Cutting force component in dry rough milling of AZ91D magnesium alloy using tools with different helix angles

Ireneusz Zagórski

i.zagorski@pollub.pl

Lublin University of Technology: Politechnika Lubelska https://orcid.org/0000-0001-6016-7011

Andrzej Weremczuk

Lublin University of Technology: Politechnika Lubelska

Monika Kulisz

Lublin University of Technology: Politechnika Lubelska

Agnieszka Skoczylas

Lublin University of Technology: Politechnika Lubelska

Research Article

Keywords: Magnesium alloy, Dry rough end down-milling, Cutting force, Composite multiscale entropy, FFT analysis, Recurrence plots

Posted Date: November 9th, 2026

DOI: https://doi.org/10.21203/rs.3.rs-11242078/v1

License: This work is licensed under a Creative Commons Attribution 4.0 International License.
Read Full License

Cutting force component in dry rough milling of AZ91D magnesium alloy using tools with different helix angles

Ireneusz Zagórski[a], Andrzej Weremczuk[b], Monika Kulisz[c], Agnieszka Skoczylas[d]

[a] Ireneusz Zagórski, Lublin University of Technology, Faculty of Mechanical Engineering, Department of Production Engineering, Nadbystrzycka 36, 20-618 Lublin, Poland; i.zagorski@pollub.pl, ORCID 0000-0001-6016-7011
[b] Andrzej Weremczuk, Lublin University of Technology, Faculty of Mechanical Engineering, Department of Applied Mechanics, Nadbystrzycka 36, 20-618 Lublin, Poland; a.weremczuk@pollub.pl, ORCID 0000-0002-0121-7100
[c] Monika Kulisz, Lublin University of Technology, Management Faculty, Department of Enterprise Organization, Nadbystrzycka 36, 20-618 Lublin, Poland; m.kulisz@pollub.pl, ORCID 0000-0002-8111-2316
[d] Agnieszka Skoczylas, Lublin University of Technology, Faculty of Mechanical Engineering, Department of Production Engineering, Nadbystrzycka 36, 20-618 Lublin, Poland; a.skoczylas@pollub.pl, ORCID 0000-0002-7707-3406

Corresponding author: Ireneusz Zagórski, i.zagorski@pollub.pl

Abstract
The study investigates the normal to the feed force component of the total cutting force in dry rough end down-milling of AZ91D magnesium alloy. The overall goal of this work is to investigate the dependence of this cutting force component on the milling parameters (particularly high cutting speeds – high-speed milling). An interesting aspect of this study pertains to the impact of end mill geometry (e.g. different helix angles) on machining effects. The study also involves capturing and analyzing the component's signal in the time domain first, and then assessing its dynamics in the frequency domain. In addition to that, the following are determined: maximum, peak-to-peak and root mean square values, along with composite multiscale entropy (CMSE) and outliers or extreme values in box plots. Also, an analysis is performed using recurrence plots, in order to assess the periodicity and continuity of the plot diagonals. Results show a clear relationship between the final CMSE value and the applied cutting speed and depth of cut. FFT analysis revealed that the signal recorded - particularly at high cutting speeds - is characterized by a significantly lower number of harmonics. The reduced complexity of the frequency spectrum indicates a potentially lower susceptibility to self-excited vibrations.

Keywords
Magnesium alloy, Dry rough end down-milling, Cutting force, Composite multiscale entropy, FFT analysis, Recurrence plots

1. Introduction

Dry rough milling of magnesium alloys currently requires a holistic approach that combines the pursuit of maximum efficiency with maintaining high quality and process stability. The implementation of high-speed machining (HSM) strategies allows for a reduction in production cycle times, which is a priority for the machinery, automotive, and aerospace industries, among

others [1]. Magnesium alloys have a high strength-to-weight ratio and low density, which makes them materials with outstanding machinability. This property allows for the effective removal of large machining allowances under high technological parameters [2, 3], as the process is characterized by significantly lower cutting forces and a more favorable thermal balance when compared to, for example, the machining of aluminum alloys [4, 5]. Specifically, cutting forces in a milling process for magnesium alloys can be approximately 50% lower than those observed for Al-Si alloys, which directly translates into significantly reduced thermo-mechanical loads exerted on the tools. The direct dependency between cutting force response and resulting surface quality has also been observed in the micro-milling of AZ31B [6, 7].

Nevertheless, the precise, finish and, naturally, rough machining of magnesium alloys entails specific physicochemical challenges. The cutting zone temperature and thermomechanical loads in dry machining require strict process control [4, 5, 8]. This issue is particularly important in dry rough milling processes for magnesium alloys, where temperature-related safety assessment and chip ignition risk must be considered together with tool geometry effects [9]. In addition, fine chips and magnesium dust must be considered from the viewpoint of ignition risk and machining safety [10]. The morphology and fragmentation of chips should also be taken into account, since they are directly related to process stability and safety in dry magnesium alloy milling [11]. In response to these difficulties, conventional water-based flood cooling is increasingly less frequently used in favor of dry machining and minimum quantity lubrication (MQL) strategies [3, 12, 13], while advanced MQL approaches, including eco-friendly nanofluid-assisted variants, have been reported to improve tribological conditions and overall machining performance [14–16]. For instance, the use of MQL in the milling of rare-earth magnesium alloys has been shown to effectively reduce the cutting zone temperature, as shown by measurements with an infrared thermography camera, and to improve surface quality compared to dry cutting [17, 18]. Moreover, mercury pool thermocouple-based measurements have demonstrated that the use of eco-friendly nanofluids, such as MoS2 nanoparticles suspended in waste oil, significantly reduces the feed component of the total cutting force and the cutting zone temperature during the machining of magnesium implants, thus presenting a biodegradable and cost-effective alternative [19].

Recent studies on sustainable machining of the AZ91D alloy under variable cutting parameters further confirm the need to balance process efficiency with force-related and quality-related responses [20]. Similar couplings between machining parameters, cutting force, chip characteristics, and tool wear have also been reported for magnesium-based composite parts [21] . Investigations on the dry face milling of short carbon fiber-reinforced AZ91 matrix composites have revealed a direct correlation between increased reinforcement content and higher cutting forces and surface roughness. This finding is consistent with the generally observed strong interrelationship between feed rate, cutting forces and surface roughness in AZ91 alloy machining [21, 22].

Furthermore, modern tool path strategies, such as helical and trochoidal milling, can markedly affect cutting stability and chip evacuation [4, 10]. This has also been confirmed in studies on AZ31 magnesium alloy, where helical milling was shown to influence both machinability and surface integrity [23]. The significance of these advanced strategies is further emphasized by the need for precise chip thickness and cutting force modeling. For instance, comparative studies on trochoidal and slot milling of aluminum alloys have shown that applying semi-mechanistic force models and matching maximum chip thicknesses can effectively minimize the discrepancies in cutting dynamics caused by different tool path conditions [24, 25].

A fundamental indicator of machinability, directly affecting process quality and safety, is the set of cutting force components. Their variability, particularly that of the feed force component F_x, influences elastic deformations in the machine tool-holder-tool-workpiece system and, consequently, affects shape accuracy and surface layer integrity [13, 26]. An initial increase in the cutting force components may decrease the undeformed chip thickness. Paradoxically, this decrease causes a subsequent rise in the forces and thus specific cutting energy, which has a negative impact on the shear angle and generates higher cutting zone temperatures [27, 28]. This phenomenon is closely related to minimum chip thickness. When the applied feed per tooth is smaller than this critical threshold, a "ploughing" effect occurs instead of cutting, leading primarily to elastic deformation. This results in unstable, increased cutting forces and a significant degradation of surface quality [29, 30].

Although increasing the feed or axial depth of cut usually leads to increased cutting forces [13, 31], these relationships are strongly nonlinear and may additionally depend on process instability [32]. Earlier studies conducted for the AZ91HP/D alloy also confirmed that both technological parameters and tool geometry significantly affect the cutting force components [33, 34]. In HSM, the cutting resistance may decrease following the process launch in the high-speed range [4, 5, 8]. Tool geometry is also crucial for stable material removal, and the helix angle in particular can substantially modify the load distribution in the cutting zone [8, 26, 31]. Similar conclusions regarding the role of helix angle in high-performance milling were reported in [35, 36]. The significant influence of cutting tool geometry on machining performance has also been confirmed in the face milling of other construction materials, where increasing the number of cutting flutes was shown to considerably reduce the components F_x and F_y and significantly improve surface roughness [37, 38]. Furthermore, cutting force components exhibit a strong dependence on the applied protective tool coatings. For instance, TiB_2 coatings have been shown to effectively minimize the F_x and F_y forces during machining light alloys (e.g. AlSi21CuNi) [39]. This was also confirmed in a study on rough milling magnesium alloys by carbide tools coated with TiAlN [40]. At highly elevated cutting speeds (exceeding 1600 m/min), these forces are also significantly influenced by the dominant tool wear mechanisms, such as adhesion and abrasion [8].

The milling environment is characterized by strong nonlinearity, where unfavorable combinations of kinematic parameters can initiate chatter, leading to a deterioration in surface quality and a decrease in repeatability [32, 41]. Under specific conditions, chatter vibrations can become so intense that their amplitude exceeds the actual chip thickness. Consequently, the chip becomes dissected or fragmented, leaving characteristic chatter marks that severely "damage" the machined surface - a phenomenon commonly referred to as machining instability. The transition from stable machining to unstable chatter is frequently governed by bifurcation phenomena, and it fundamentally alters the nonlinear milling dynamics [42]. The determination of stable condition limits and the avoidance of resonances have so far relied mainly on stability lobe diagrams [43, 44]. However, the classical FFT-based analysis is often insufficient for the interpretation of non-stationary signals [45]. Therefore, it is increasingly complemented by nonlinear dynamics methods, such as recurrence plots [46, 47] and composite multiscale entropy (CMSE), which enable a more precise assessment of transient phenomena and signal disorder [48, 49]. In such cases, alternative signal-processing approaches, including wavelet-based and Hilbert–Huang methods, may provide a more detailed description of transient changes in cutting-force signals [50]. Recurrence plots together with recurrence quantification analysis (RQA) have proven to be remarkably effective advanced nonlinear methods for

analyzing cutting force time series. They allow for the detection of subtle dynamic changes, process instabilities, and even minor surface defects [51].
The interpretation of multi-parameter milling results is often complemented with an analysis of variance (ANOVA), which enables the determination of statistical significance of both technological parameters and tool geometry on the components of the total cutting force [52, 53]. Apart from ANOVA, the advanced prediction of cutting force components and material damage based on technological parameters can be effectively performed using Artificial Neural Networks which have demonstrated a strong predictive capability for cutting forces and delamination-related indicators [54, 55]. In the context of dry rough milling of magnesium alloys, such statistical approach helps compare machining conditions and indicate parameter ranges associated with a greater process stability and a lower likelihood of process-related defects.
Despite the growing knowledge base regarding magnesium alloys machinability, the literature still lacks comprehensive analyses correlating high-speed machining parameters with the nonlinear dynamics of end mills with different edge geometries (e.g. helix or rake angles). A recent work investigating a dry rough milling process for alloy AZ31B conducted with tools of different geometry also confirmed the strong relationship between tool geometry, vibration response and process stability [56].
In response to this gap, the present work studies the behavior of the normal to the feed force component F_x during a dry rough down-milling process for alloy AZ91D that is conducted with two different tools having their helix angle set equal to 20° and 50°, respectively. The study covers not only the amplitude (maximum values, peak-to-peak, RMS) and the scatter of force results using box plots, but also the signal complexity using CMSE methods, FFT spectra, and recurrence plots. The culmination of the work is a comprehensive stability assessment using ANOVA tests, which served to develop specific guidelines on safe and efficient milling of this alloy.

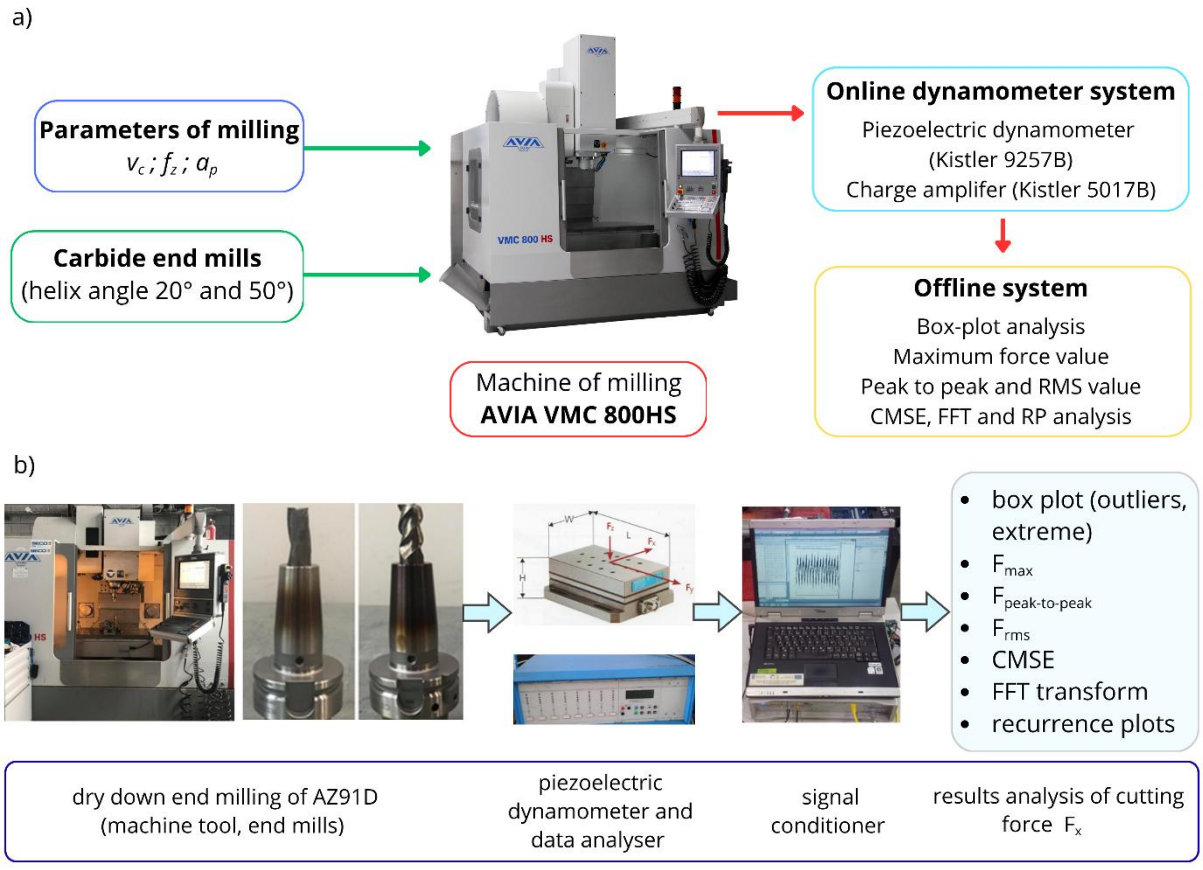
2. Methods and materials

The research was conducted on the specimens of AZ91D magnesium die-casting alloy, with its main alloying elements being aluminum, zinc, and manganese. Experiments were carried out under high-speed machining conditions on a vertical high-speed machining center, Avia VMC 800 HS, which is specifically designed for light alloy machining. Due to high values of the chip cross section, this process can also be classified as high-performance cutting (HPC). The milling process was performed using three-flute uncoated carbide end mills. The tools had different helix angle geometries (λ_s of 20° and 50°), and they were mounted in shrink fit toolholders and balanced (on a balancing machine Cimart RT610) as specified in the ISO 21940-11:2016 standard for grade G2.5 (up to 25,000 rpm). Figures 1a and 1b show the experimental setup and measuring equipment in the end-milling process under study.
A statistical analysis was performed to determine the significance of the applied parameters of milling (cutting speed v_c, feed per tooth f_z, and depth of cut a_p) on the F_x component. First of all, the Shapiro-Wilk W test was employed to test the normality of distribution. It showed that not all of the studied variables had normal distributions. These were: F_x for v_c = 800 m/min and λ_s = 50° (W = 0.7830; p = 0.0187) and a_p = 3 mm and λ_s = 50° (W = 0.8224, p = 0.0495). Since the lack of normality prevented the use of a parametric test, a non-parametric test developed by Kruskal-Wallis was employed, followed by a multiple comparison of mean ranks for all dependent variables. For the variables that followed a normal distribution, the homogeneity of

variances was examined by Levene's test. Unfortunately, the variances of all examined variables with normal distributions were heterogeneous, which precluded the use of a one-way ANOVA. For such cases, Welch's ANOVA was applied, because it does not require the assumption of equal variances to be met. To demonstrate statistically significant differences between the effect of the analyzed technological parameters on the cutting force component F_x, a Games-Howell test was performed. This is a parametric post-hoc test that is used after ANOVA if the assumption of homogeneity of variances is not met. The significance level in all statistical analyses was set to $\alpha = 0.05$. A diagram showing the applied methodology of statistical analysis is given in Figure 1c, while Table 1 lists all types of tests used for a statistical analysis of the studied dependent variable F_x. All statistical analyses were performed using Statistica ver. 13.

Table 1. Types of tests used for a statistical analysis of the dependent variable F_x for different milling conditions

F_x versus v_c for λ_s=20°	ANOVA Welch
F_x versus v_c for λ_s =50°	Kruskal-Wallis
F_x versus a_p for λ_s =20°	ANOVA Welch
F_x versus a_p for λ_s =50°	Kruskal-Wallis
F_x versus f_z for λ_s =20°	ANOVA Welch
F_x versus f_z for λ_s =50°	ANOVA Welch



c)

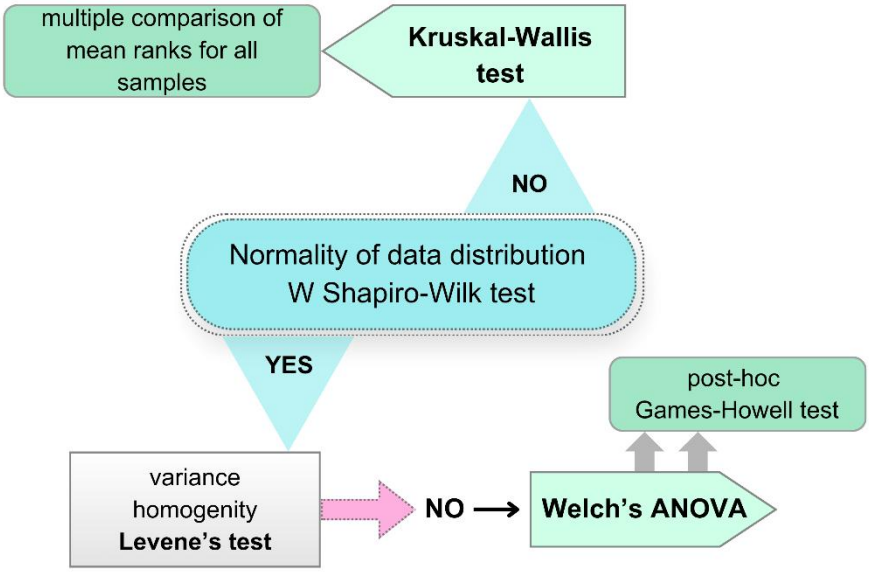


Figure 1. Schematic research diagram methodology: a) research flowchart, b) experimental setup for conducting dry end milling tests and measuring cutting forces, c) methodology for ANOVA statistical analysis of results

To compare these results with the findings of earlier studies in this field, the main technological parameters of milling were made variable. The radial depth of cut a_e was maintained constant throughout the milling process and set equal to 14 mm. This value was selected in compliance with the recommendation of cutting tool manufacturers, who suggest that for stable milling this depth value should be below 25% of the tool diameter or above 75% of the tool diameter. Table 2 lists all machining technological parameters (both variable and constant).

Table 2. Results of Welch's one-way ANOVA regarding the influence of cutting speed (v_c), depth of cut (a_p), and feed per tooth (f_z) on the F_x component of the total cutting force, where: df1 - degrees of freedom for the variance between groups, df2 - degrees of freedom for the variance within groups, F - value of the test statistic, p - probability level.

Variable parameters	Constant parameters
v_c from 400 to 1200 m/min	f_z 0.15 mm/tooth, a_p 6 mm, a_e 14 mm
f_z from 0.05 to 0.30 mm/tooth	v_c 800 m/min, a_p 6 mm, a_e 14 mm
a_p from 0.5 to 6.0 mm	v_c 800 m/min, f_z 0.15 mm/tooth, a_e 14 mm

All cutting force components were measured with a piezoelectric dynamometer from Kistler (model 9257B) and a 5017B amplifier. As a result, it was possible to capture sequences of signals for the variable milling parameters, for the established time series. Given the great quantity of captured data, this study investigates only one component of the total cutting force, namely – the one measured in the X-direction, F_x, also known as the component normal to the feed force, F_{fn} (other components of the total cutting force that could be captured included: F_y – feed force component F_f, and F_z – passive force component F_p). The sampling frequency was 10 kHz. Thanks to the use of Kistler's dynamometer, all cutting force components could be measured with a ±5 kN accuracy range.

All captured signals of the F_x component were examined, except those at the tool's entry and exit from the workpiece, so as to enable a comparative analysis of the research data. Maximum, peak-to-peak, and root mean square (RMS) values were among the cutting force indicators under analysis. Additionally, the study's findings were displayed as box plots, which, among other things, made it possible to see outliers and extreme values. Furthermore, all results were

processed by composite multiscale entropy (CMSE), which was calculated using Matlab's normal, regular approach [48, 56]. The CMSE calculation takes advantage of coarse-graining, wherein thereby obtained time series is used as an average of the original data points in non-overlapping windows by increasing a scale factor of τ. Every coarse-grained time series has a length of N⁄τ. From a practical perspective and according to literature sources, when $\tau < 20$, the error is very small and has no effect on the accuracy of the calculated CMSE value. Thus, the scale factor τ was also included in the calculation.

3. Results

The parameters and conditions of milling were chosen on a basis of a previous analysis of stable machining regions [56] and earlier studies, as well as a review of the literature in this field. Cutting force component signals were captured in dry rough end-milling conducted with variable machining parameters. An example of a cutting force component F_x time series in a dry end milling process is shown in Figure 2.

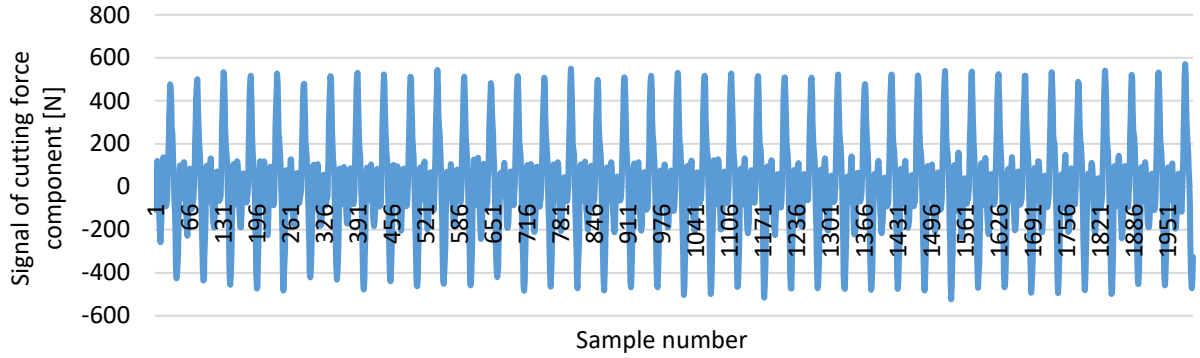


Figure 2. Example of a cutting force component F_x signal recorded in a milling process conducted with: v_c 600 m/min, f_z 0.15 mm/tooth, a_p 6.0 mm, a_e 14 mm (helix angle 50°)

The following signals of the F_x component were analyzed: the maximum value, peak-to-peak value, root mean square (RMS) value, along with outliers or extreme values in the box plots. Also, the box plots show the scatter of the results. In addition to providing valuable information about the machining process, these plots also show the location of results (time series). The recorded signals of this component have very similar patterns in the time series; however, their ranges and values differ.

The box plots predominantly show the dependence of the variable technological parameters (v_c, f_z, a_p) on the two different tools. Each box plot comprises the following [56]: box – contains the standard deviation, whiskers – present the scatter of the results (maximum and minimum values), outliers and extreme – show the values outside the max-min range as round points and asterisks. The remaining experimental data are plotted as bar diagrams showing the maximum, peak-to-peak, and root mean square (RMS) values. Linear plots show the results of composite multiscale entropy (CMSE) calculations. Next, FFT analysis results are presented, which identify the dominant frequencies in the signal. Finally, recurrence plots (RPs) are given to illustrate the periodicity of the analyzed force signals. The maximum value of the F_x component was defined as the average of its 10 maximum values. This allowed, on the one hand, for the presentation of the maximum value and, on the other, for the visualization of the scatter of the maximum values by adding the standard deviation. The peak-to-peak value was calculated as the difference between the maximum and minimum values of the F_x component. The RMS value of this force component was calculated using the standard procedure, e.g., [52,56].

3.1.Box plots, maximum cutting force, peak-to-peak, root mean square value

Box plots were created to analyze the scatter between obtained cutting force results. Figure 3 shows the dependence of the cutting speed and helix angle on the cutting force component F_x. One can observe that, for most cases, the machining process proceeds under stable conditions, without the occurrence of values classified as outliers or extreme. Isolated outliers only occur when machining is conducted using cutting speeds of 600–800 m/min and a helix angle of 50°. This may indicate reduced stability of milling under these particular conditions. Furthermore, in the high-speed machining range (especially at 1200 m/min), the values of the F_x component become stable and decrease, which is desirable directly due to lower force values and indirectly due to probably lower cutting zone temperatures (lower forces should generate lower temperatures). A comparison of the two helix angle values, however, reveals - in some cases - higher standard deviations for a helix angle of 50°; in the remaining cases, the values are comparable. The values shown in Figure 3 are within a fairly wide range from approx. 300 N to approx. 700 N.

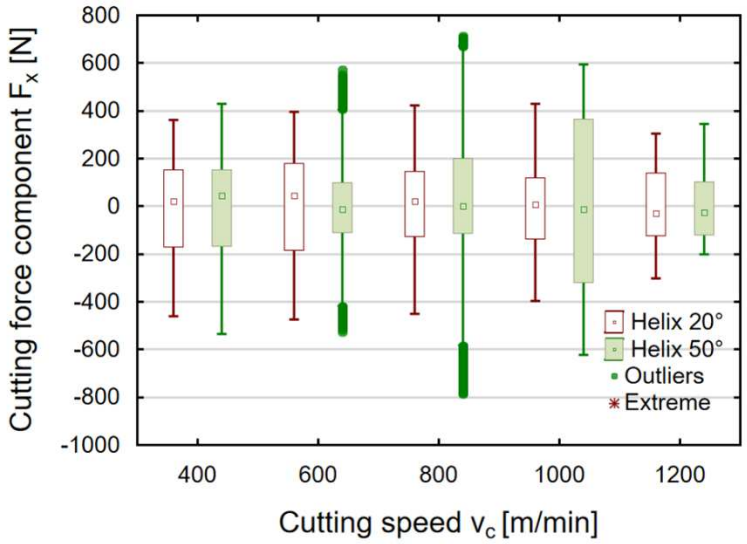
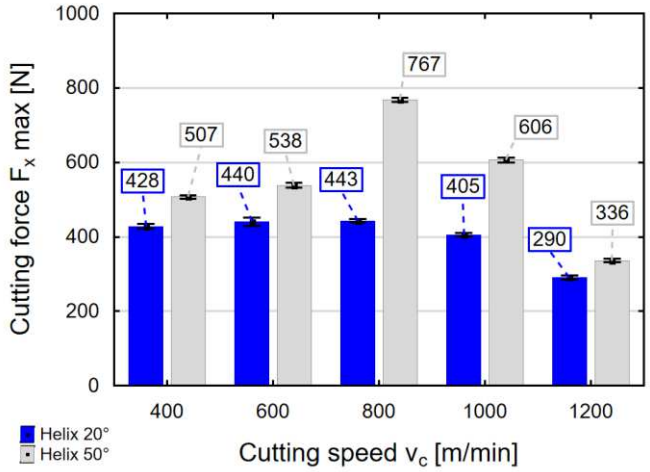


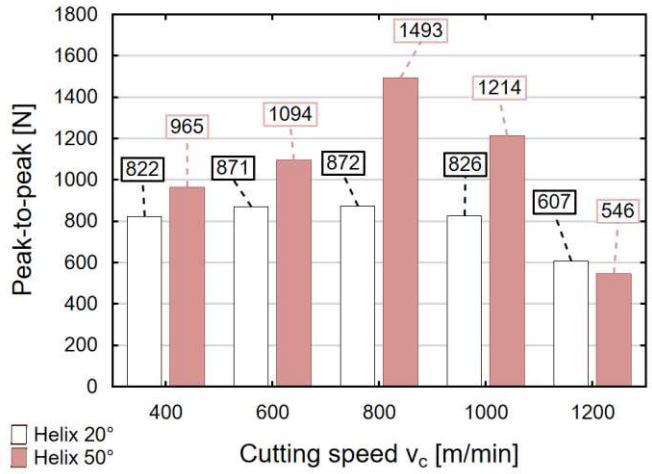
Figure 3. Cutting force component F_x (in a box-plot form) for different helix angles and variable cutting speed v_c

Subsequent plots (Figure 4) present component F_x metrics such as maximum value (F_{xmax}), peak-to-peak, and root mean square value. These results relate to the variable cutting speed, which also included the high-speed machining range. The maximum value and the range of variation (peak-to-peak) of the component increase up to a cutting speed of 800 m/min, after which these values decrease, especially at 1200 m/min. The speeds between 1000 and 1200 m/min can be defined as the high-speed machining range. After exceeding the conventional cutting speed limit, the component values (including the maximum, peak-to-peak, and root mean square values) begin to decrease, reaching their minimum at the maximum cutting speed. This is a beneficial effect of machining conducted at elevated cutting and rotational speeds. Furthermore, these results (for the maximum value of the component) are characterized by a relatively low standard deviation. Such machining is primarily possible for light alloys (aluminum and magnesium) when using high-speed electric spindles. The observed maximum values under high-speed machining conditions fluctuate around approximately 300 N. A

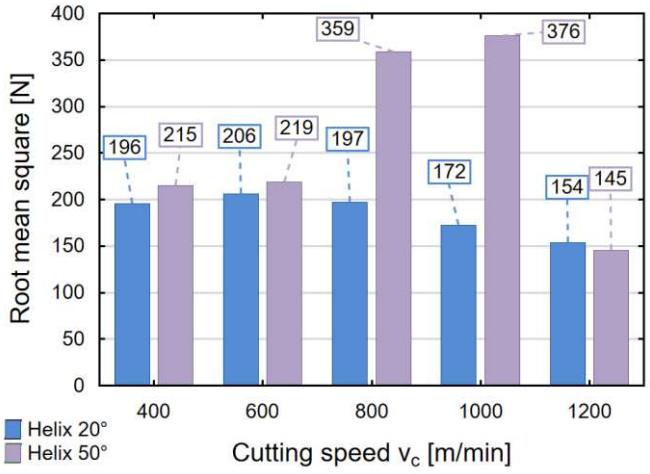
comparison of these values to those observed in machining at 400 m/min reveals a favorable decrease in the component value, by approximately 140–170 N relative to the initial value. A similar, though not exactly the same, situation can be observed for RMS. For this case, the highest values are observed in the following speed ranges: 600–800 m/min for the tool with a helix angle of 20° and 800–1000 m/min for the 50° tool. For both cases, the most favorable conditions occur at 1200 m/min. The RMS values observed at this speed are the lowest across the entire machining range, amounting to approximately 154 N and approximately 145 N, respectively.



a)



b)



c)

Figure 4. Cutting force component F_x for different helix angles and cutting speeds: a) maximum value, b) peak-to-peak, c) root mean square (RMS)

Another box plot (Figure 5) shows the dependence of feed per tooth and helix angle on the cutting force component F_x. One can notice here is a greater scatter of the results than that observed for cutting speed. This is particularly evident for a wide range of feeds, namely from 0.10 to 0.25 mm/tooth. Interestingly, this relationship occurs only for the 50° tool. Again, like in the case of cutting speed results, a greater scatter between the test results occurs for the 50° tool. A change in the feed value causes an increase in the chip cross-section, which directly affects both the values and the results scatter, as analyzed by evaluating the cutting force component. The values shown in Figure 5 range widely from approximately 200 N to approximately 800 N. Despite the high values of the component, a certain stabilization of these force component values can be observed for the feed value ranging from 0.20 mm/tooth to 0.30 mm/tooth. Given the efficiency of this process, it is therefore recommended that machining be conducted with medium feed rates, thereby achieving, on the one hand, increased machining efficiency at low feeds, while, on the other, preventing an excessive increase in the results scatter for this cutting force component.

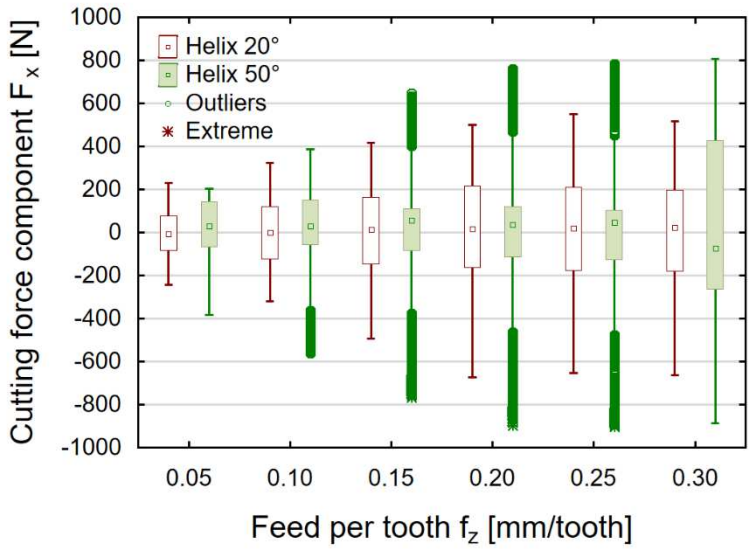
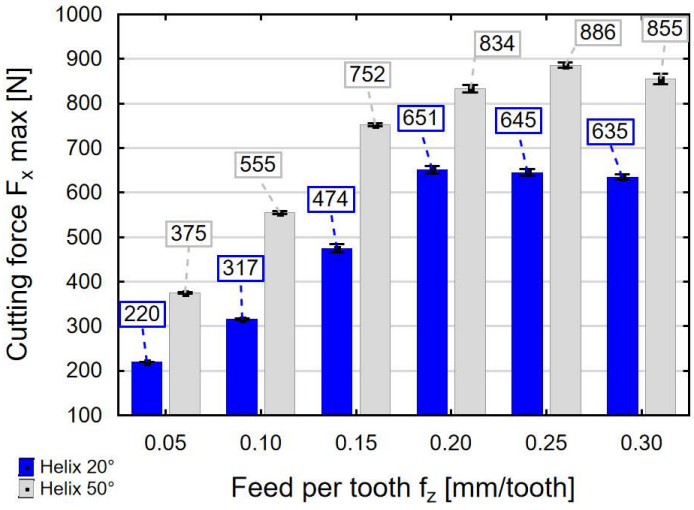
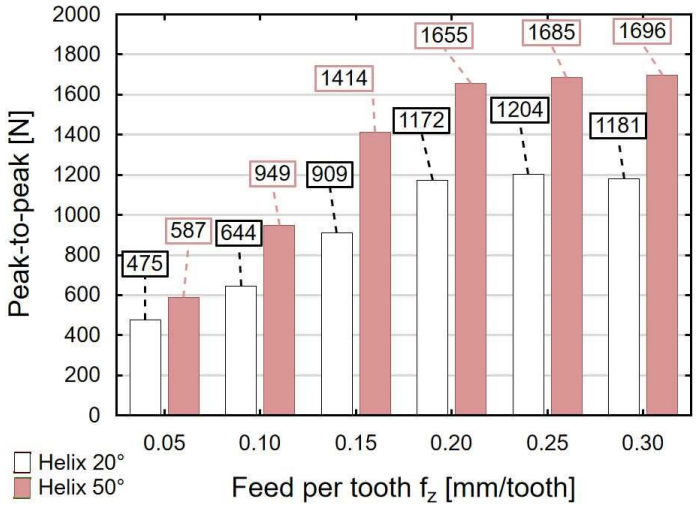


Figure 5. Cutting force component F_x (in a box-plot form) for different helix angles and variable feed per tooth f_z

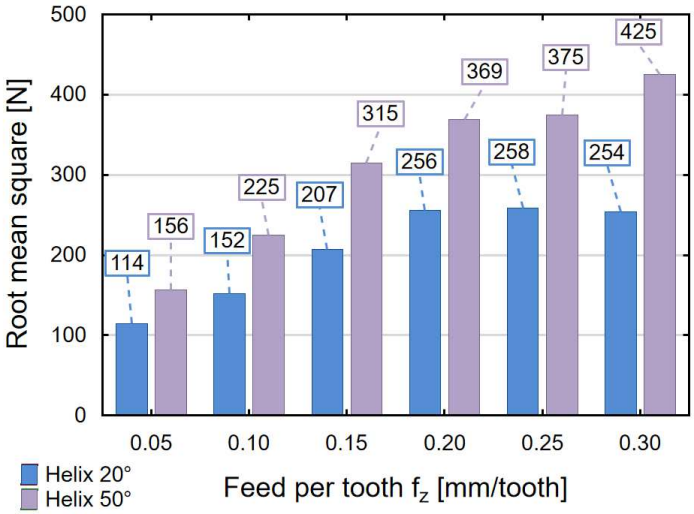
An analysis of the feed per tooth results (Figure 6) reveals the expected increase in individual measures characterizing the cutting force component F_x. The maximum value of the F_x component increases from 220 N to 375 N for a feed per tooth value of 0.05 mm/tooth (for the helix angles of 20° and 50°, respectively), to approximately 635–651 N and approximately 834–886 N for the feed range of 0.2–0.3 mm/tooth (for the angles 20° and 50°, respectively). Similar relationships can also be established for measures such as the peak-to-peak and RMS values. In the case of peak-to-peak, the range of changes is between approx. 475 N and approx. 1204 N (for the helix angle 20°), and from approx. 587 N to 1696 N (for the helix angle 50°). The RMS value changes as follows: from approx. 114 N to approx. 258 N (helix angle 20°), and from 156 N to approx. 425 N (helix angle 50°). Once again, lower values of the component were produced during machining conducted with the 20° tool.



a)



b)



c)

Figure 6. Cutting force component F_x for different helix angles and feeds per tooth: a) maximum value, b) peak-to-peak, c) root mean square (RMS)

The last box plot (Figure 7) describes the interrelation between the axial depth of cut, helix angle and cutting force component F_x. This relationship is analogous to that established for feed per tooth. A higher depth of cut (and thus in the chip's cross-section) causes an increase in the

F_x values and the scatter of the results. For this case, the results range from approximately 100 N to the values observed for feed and cutting speed, i.e., approximately 800 N. Once again, most of the results classified as outliers and extreme are achieved for the 50° tool. Only for a feed rate of 0.30 mm/tooth and a helix angle of 20° can one observe the presence of results classified as outliers and extreme. It is quite evident, that machining conducted with high a_p values can cause local increases in the cutting force value and in the scatter between these values. Once again, for most cases, the machining process performed by the 50° tool was characterized by higher values and wider range of F_x.

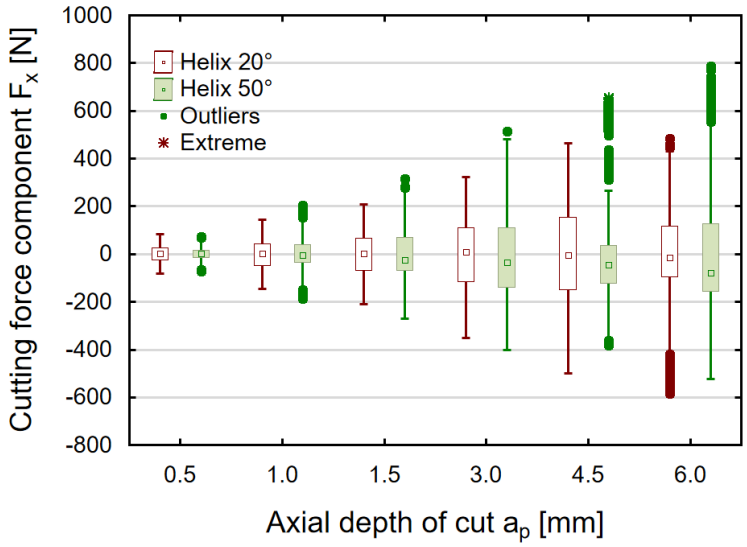
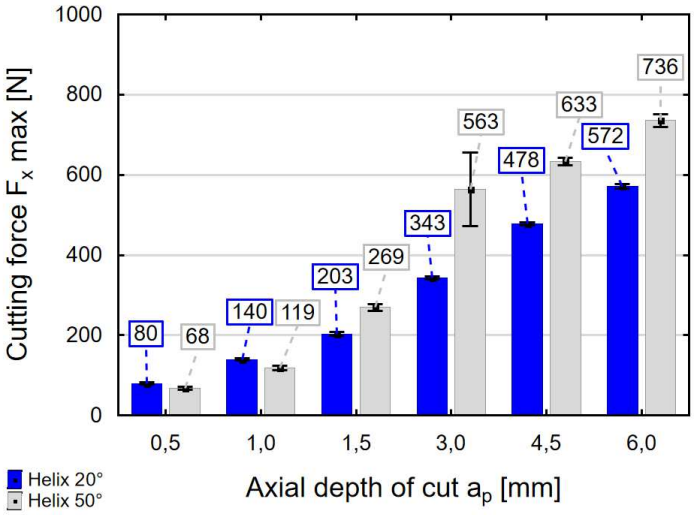
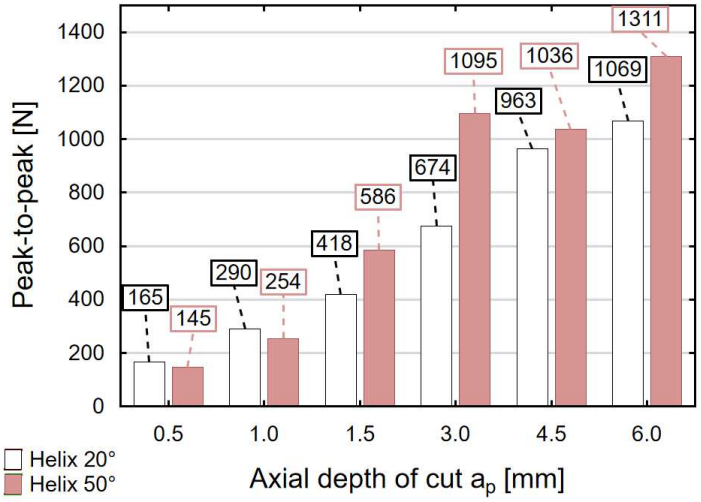


Figure 7. Cutting force component F_x (in a box-plot form) for different helix angles and variable axial depth of cut a_p

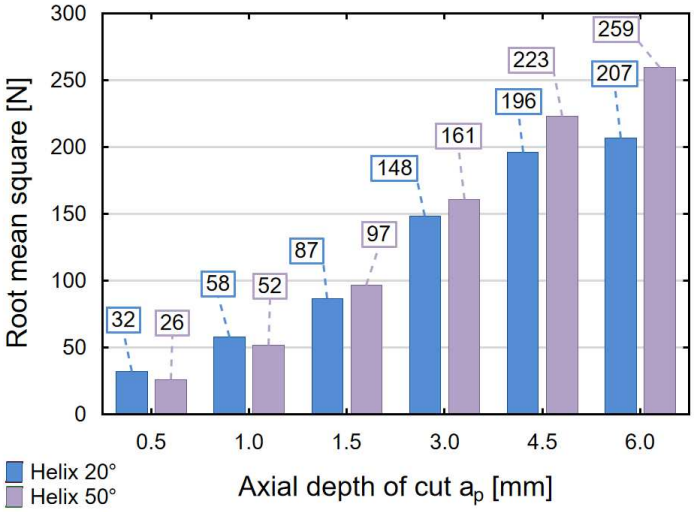
The final anlaysis of axial depth of cut dependency is plotted in Figure 8. Similarly to feed per tooth, an increased depth of cut increases the cutting force component. For a_p ranging from 1.5 mm to 6 mm, higher component values are observed for the helix angle 50°. Furthermore, for this tool, a fairly large results scatter is observed at $a_p = 3.0$ mm. The component values range from 80 N to approx. 570 N (helix angle 20°), from approx. 70 N to approx. 740 N (helix angle 50°)—for the maximum value; from 165 N to 1069 N (helix angle 20°), from approx. 145 N to approx. 1311 N (helix angle 50°) – for the peak-to-peak value; from approx. 30 N to approx. 200 N (helix angle 20°), and from 26 N to approx. 260 N (helix angle 50°) – for the root mean square value. It can be assumed with some simplification that the component remains at a relatively low level for the axial depth of cut ranging from 0.5 to 1.5 mm. In contrast, the use of higher a_p values, which are very characteristic of roughing, results in high F_x values, ranging from approx. 340 N to approx. 570 N and from approx. 570 N to approx. 740 N (for the helix angles 20° and 50°, respectively, and for the maximum value of F_x).



a)



b)



c)

Figure 8. Cutting force component F_x for different helix angles and axial depths of cut: a) maximum value, b) peak-to-peak, c) root mean square (RMS)

3.2.Composite multiscale entropy

The F_x component signals measured in the experiments were also processed by multiscale composite entropy (CMSE). This method allows for the dynamics of the experimentally obtained signals to be examined. The calculated value of entropy describes the degree of disorder in the measured signals, thus defining their dynamic complexity. Results of the analysis by this method are presented in Figs. 9-14.

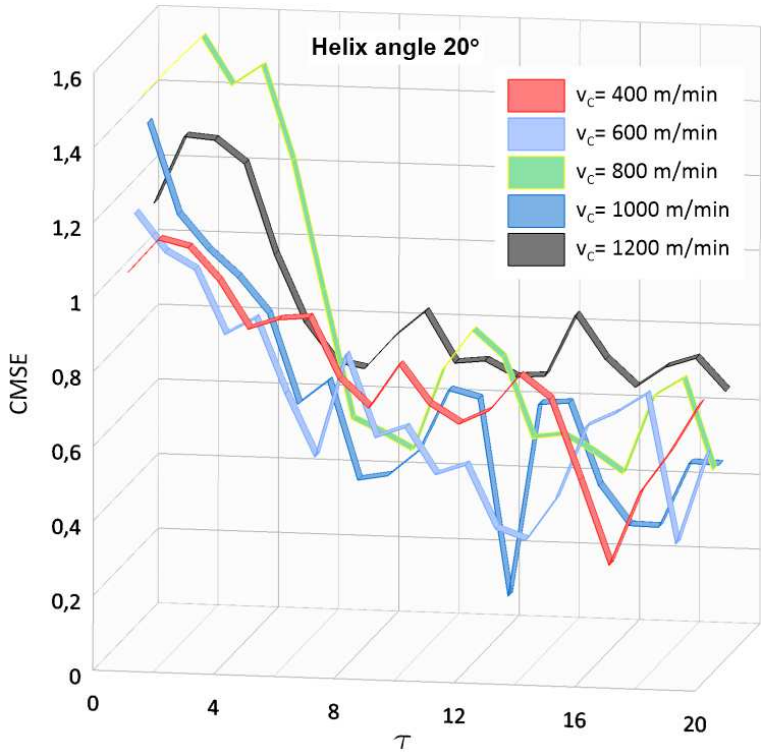


Figure 9. CMSE values of F_x for helix angle 20° and different cutting speeds

First, using the CMSE procedure, the value of a coarse-grained time series y(τ) was calculated for a scale factor τ by a one-dimensional time course x with a total length of N. After that, the sampling entropy SampEn was determined to define the probability whether two consecutive data strings of length m would be similar to each other within a tolerance of r. The CMSE value was calculated by averaging of τ SampEns. The string length m = 2 and the scale factor τ = 20 were used for the calculations. The tolerance r was chosen to be 10% of the standard deviation of the original time series. The Matlab Simulink 2019b software and widely available formulas and equations were used for the calculations.

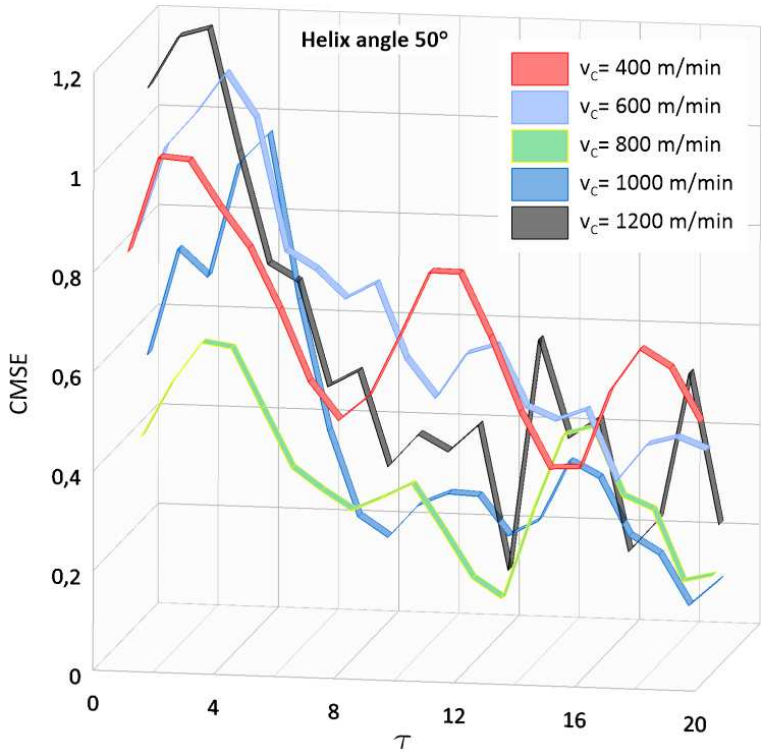


Figure 10. CMSE values of F_x for helix angle 50° and different cutting speeds

Figure 9 shows CMSE results for the F_x component signals that were captured during milling conducted by the 20° tool at different cutting speeds. In the initial range of parameter τ (τ < 6), the highest entropy value was observed at v_c = 800 m/min. At higher values of parameter τ, the entropy level became equal for all tested cutting speeds. For the 50° helix angle tool (Figure 10), the highest entropy values were observed at v_c = 1200 m/min in the initial range of parameter τ. The lowest entropy values across the entire τ parameter range were observed at v_c = 800 m/min. This indicates a significantly lower dynamics of the milling process when the above tool and cutting speed are used. At the same time, comparing both tools, lower entropy values can be observed in machining conducted with the 50° helix angle tool for all analyzed cutting speeds. Based on this, it can be concluded that using this tool is more advantageous due to the lower complexity of the cutting dynamics.

Next, the effect of feed per tooth was analyzed. For a helix angle of 20° (Figure11), the lowest entropy values were obtained for the lowest feed per tooth. The entropy calculation results for the remaining feeds per tooth did not show significant differences. The exception was the entropy level for f_z = 0.1 mm/tooth and τ>15. In this range, the entropy value was significantly higher at the indicated feed per tooth compared to the other results. For a helix angle of 50° (Figure 12), an increase in the feed per tooth made the entropy level increase, too. The feed increase was proportional, and this trend was observed for all tested feeds per tooth. For the variable feed per tooth, lower entropy values were also observed when using the 50° tool.

When examining changes in the axial depth of cut, similar entropy values were observed, regardless of the tool used (helix 20° - Figure 13, helix 50° - Figure 14). Smaller differences between the calculated entropy values were observed for the 20° tool. For both cases, the entropy value decreased to a considerable extent with increasing the axial depth of cut.

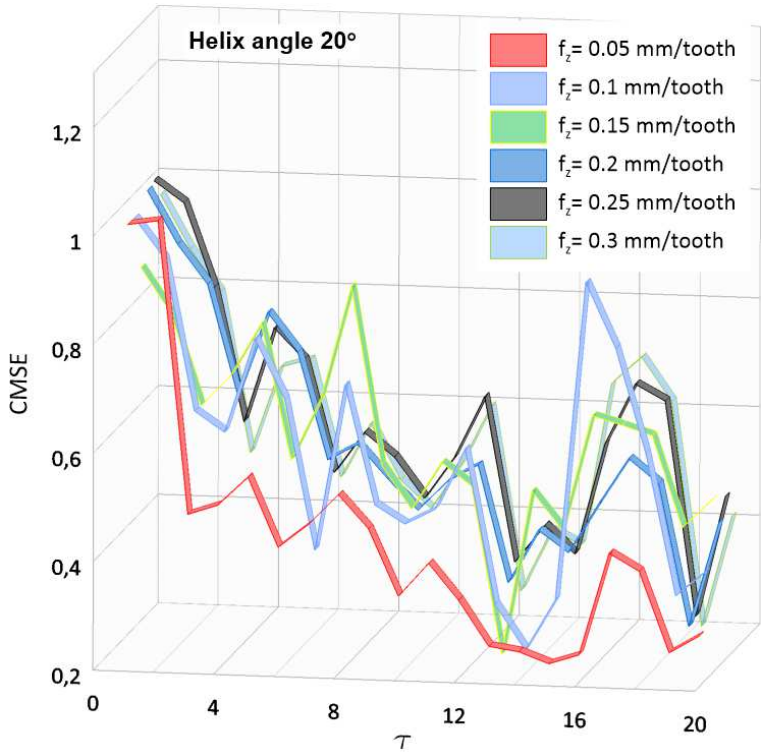


Figure 11. CMSE values of F_x for helix angle 20° and different feeds per tooth

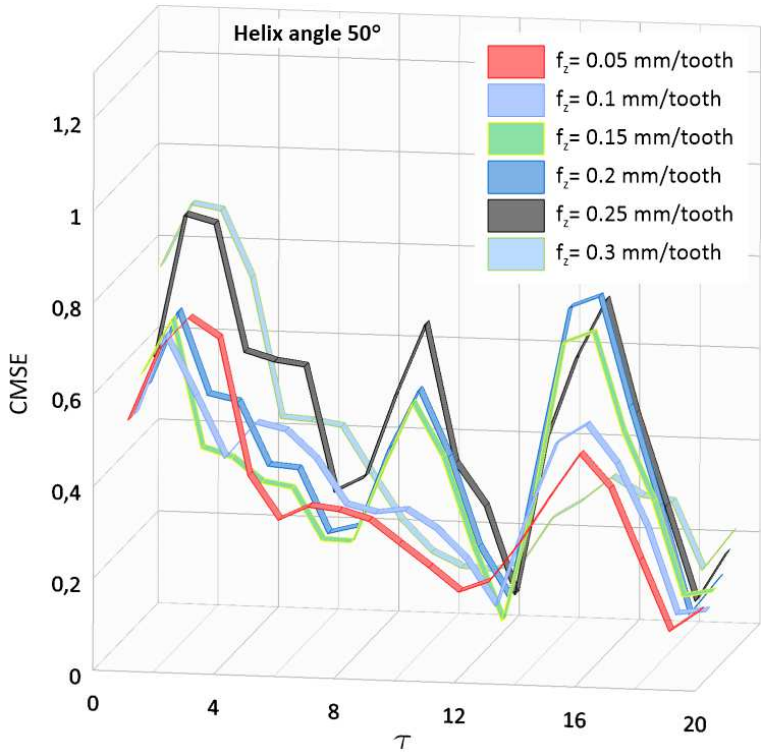


Figure 12. CMSE values of F_x for helix angle 50° and different feeds per tooth

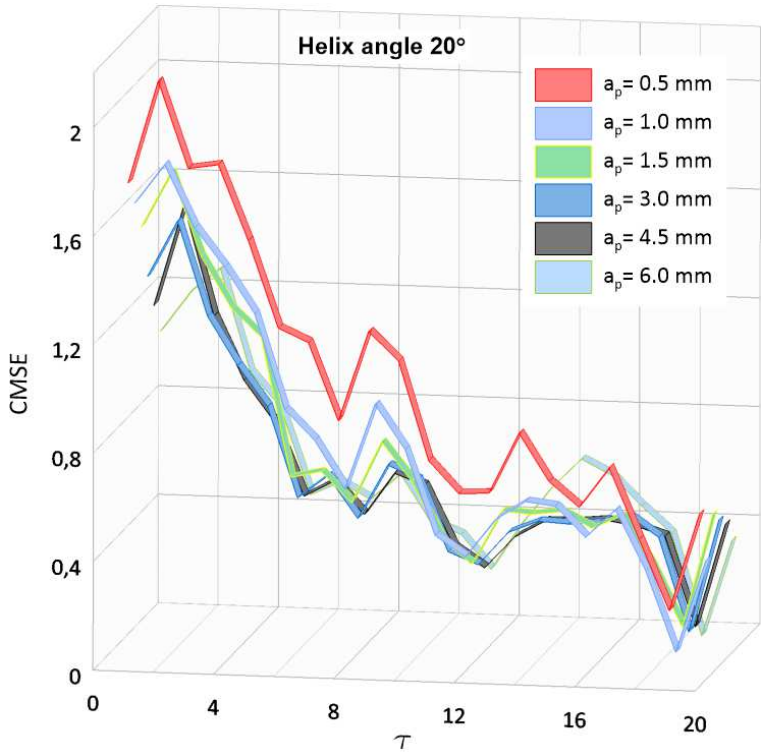


Figure 13. CMSE values of F_x for helix angle 20° and different axial depths of cut

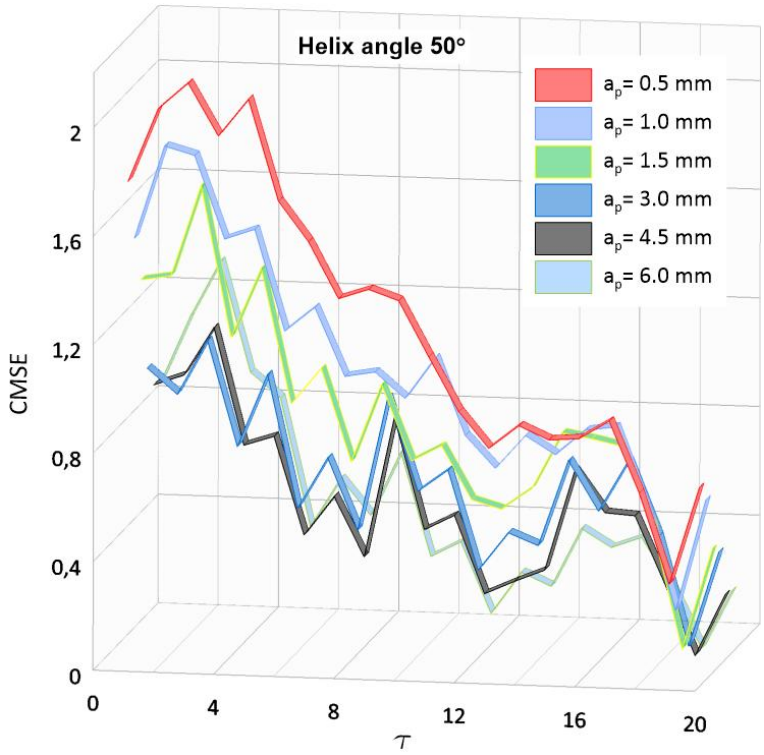


Figure 14. CMSE values of F_x for helix angle 50° and different axial depths of cut

3.3.Fast Fourier Transform Analysis

The cutting force component F_x signals captured in the experiments were analyzed in the frequency domain by the Fast Fourier Transform (FFT). This approach made it possible to

determine the frequency of the F_x component. All calculations were made with a Matlab R2019b algorithm. This helped detect self-excited vibration (chatter), the occurrence of which complicates and significantly impedes the milling process. The analysis was performed for the cutting force component F_x signals that were measured for variable milling parameters (v_c, f_z, and a_p) and different geometry tools.
Characteristic peaks visible in the FFT graphs define individual frequencies of the analyzed F_x component signals and their harmonics. The number of harmonics and their amplitudes can be used to measure the degree of complexity of the signal, and thus the complexity of its dynamics. The higher the number of harmonics is, the stronger the likelihood of their overlapping and amplifying becomes. The characteristic peaks in the FFT graphs primarily result from the operation of individual cutting flutes and their interaction with other vibration sources. This can lead to the occurrence of unfavorable self-excited vibrations during milling.

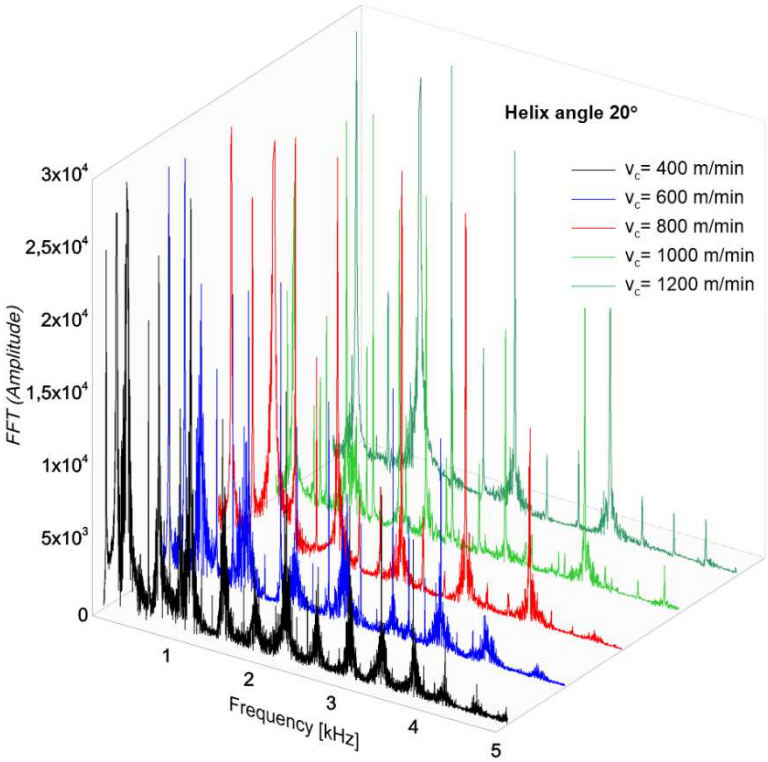


Figure 15. FFT for cutting force component F_x for a helix angle of 20° and different cutting speeds

First of all, the influence of variable cutting speed was examined. Obtained results are presented in Figure 15 (for helix angle 20°) and in Figure 16 (for helix angle 50°). For both cases, one can observe that the number of harmonics decreases and their values become significantly lower with increasing the cutting speed. This effect is particularly visible when milling is conducted with v_c = 1200 m/min using 50° tool (Figure 16). This is a beneficial phenomenon, as a lower number of harmonics significantly reduces the likelihood of unfavorable self-excited vibrations occurrence during machining.

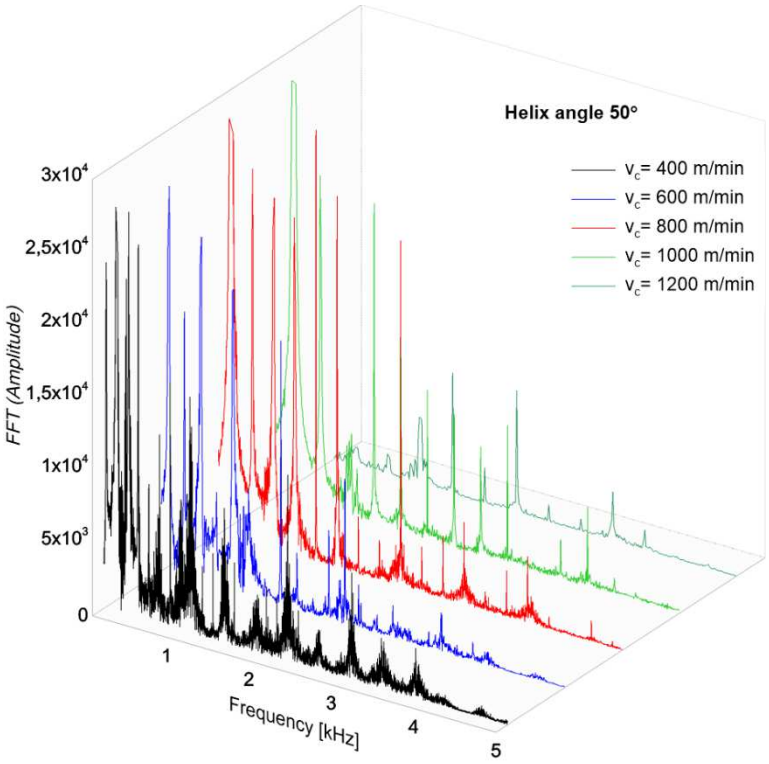


Figure 16. FFT for cutting force component F_x for a helix angle of 50° and different cutting speeds

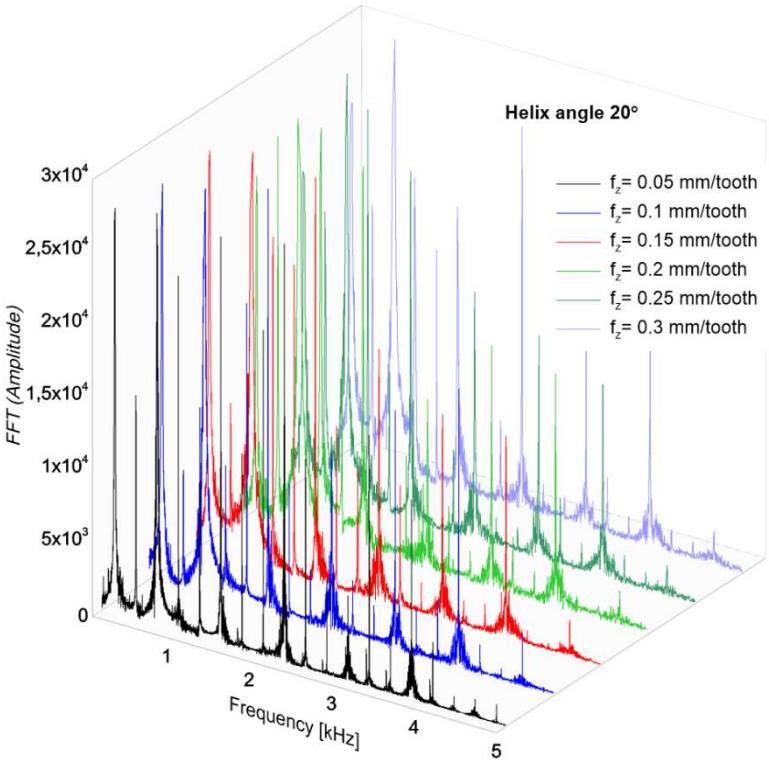


Figure 17. FFT for cutting force component F_x for a helix angle of 20° and different feeds per tooth

A higher feed per tooth value induces a gradual decrease in the number of harmonics in the analyzed signal spectrum (Figure 17 and Figure 18). A smaller number of harmonics, especially

in the higher frequency range, was observed when the machining process was conducted using the 50° tool. The fewest number of harmonics was observed at f_z = 0.25 mm/tooth.

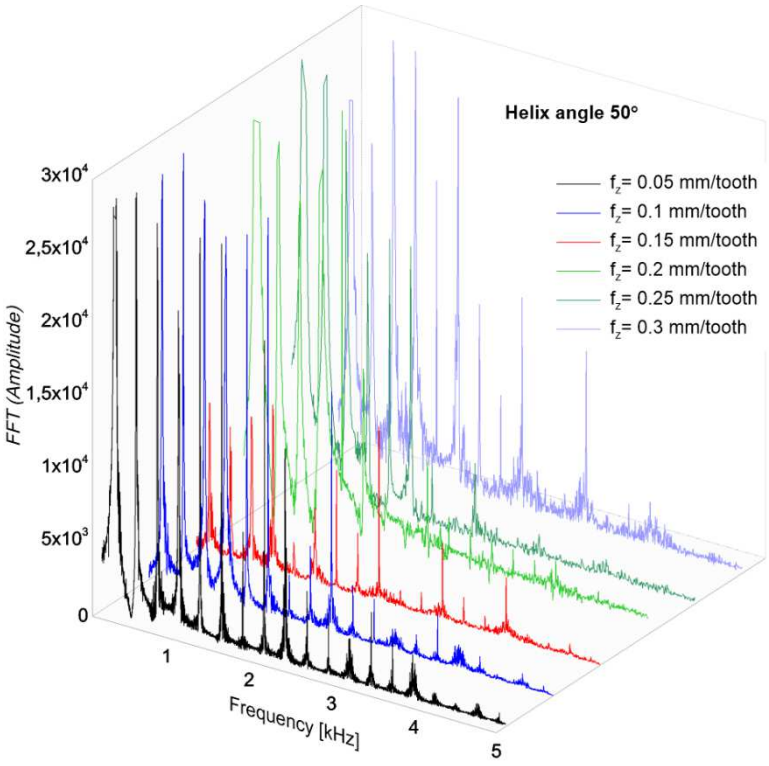


Figure 18. FFT for cutting force component F_x for a helix angle of 50° and different feeds per tooth

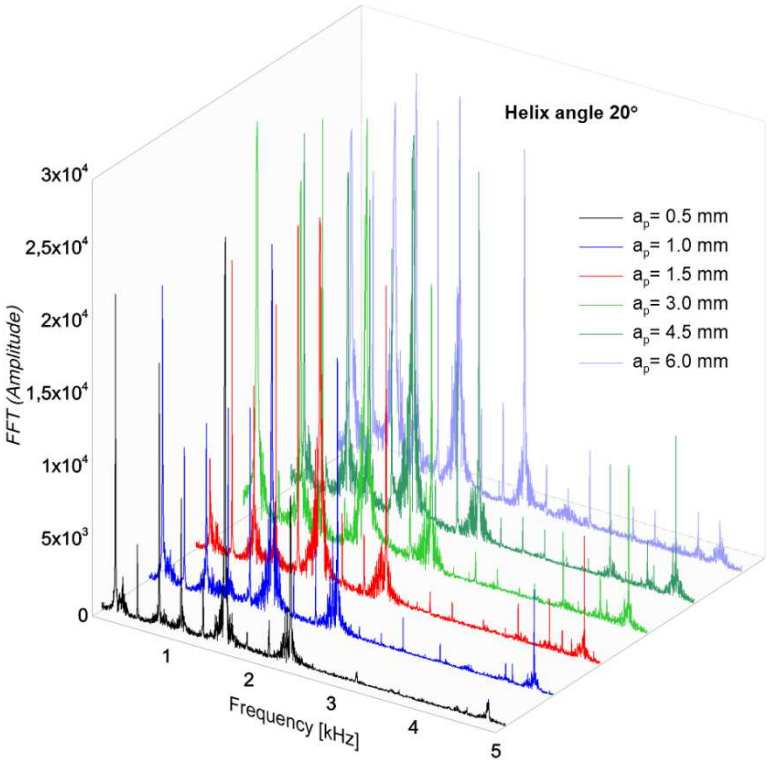


Figure 19. FFT for cutting force component F_x for a helix angle of 20° and different axial depths of cut

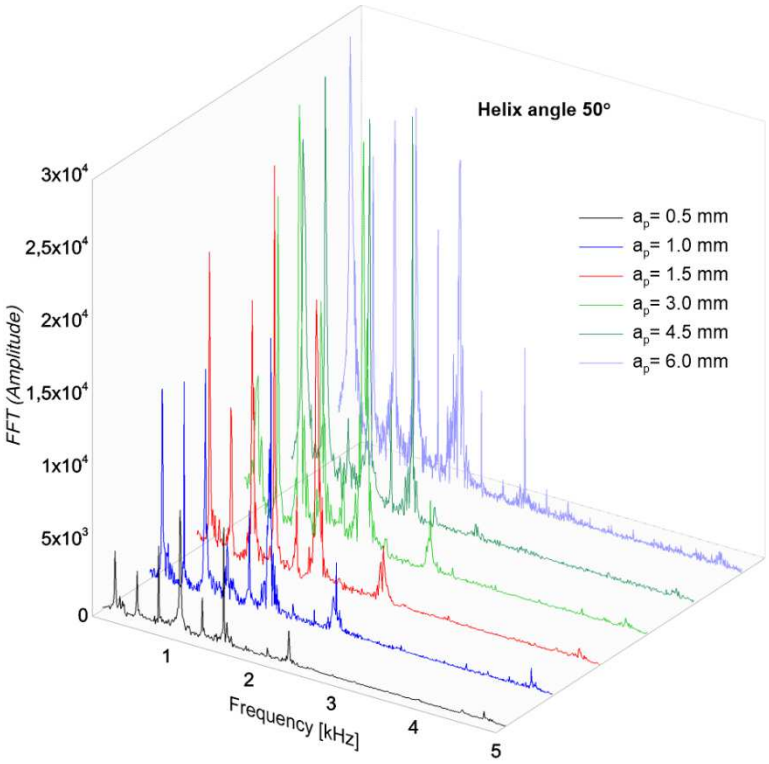


Figure 20. FFT for cutting force component F_x for a helix angle of 50° and different axial depths of cut

The greatest changes in the signal spectrum were observed when milling was conducted with variable axial depth of cut using both types of tools (Figure 19 and Figure 20). For the 20° tool, above 2.5 kHz occurs a sharp decrease in the number of harmonics and their amplitude, especially in the range of smaller axial depths of cut (Figure 19). Even better results were achieved for the 50° tool. Above 2.5 kHz, for all analyzed axial depths of cut, the occurring harmonics have a marginal effect on the signal dynamics. Therefore, milling with the 50° helix angle tool is more advantageous.

3.4.Recurrence Plots Analysis

A classical analysis of the cutting force components can adequately reveal complex signal dynamics. Therefore, a nonlinear recurrence analysis method was proposed, which yielded very promising results in a broad analysis of the dynamics of various measurement signals. Every recurrence plot was generated using 700 data points. The same embedding parameters were used, i.e., $m = 5$ and $\tau = 6$. The threshold ϵ was set to 0.75 times the standard deviation. In this analysis, the plots are presented in such a way that the upper panel shows the normalized signal correlated with the recurrence plot (lower plot).
Figure 21 presents recurrence plots obtained for the force signals captured at the extreme tested cutting speeds (v_c = 400 m/min and v_c = 1200 m/min) for both tools (helix angles 20° and 50°). Periodic vibrations were observed, characterized by very long diagonals running parallel to the mean diagonal. A direct correlation is evident between the cutting speed and the spacing between the diagonal lines. Increasing the cutting speed reduces both the force signal period and the spacing between these lines. At lower cutting speeds, the diagonal lines seem parallel yet show additional fluctuations, which is demonstrated by the time histories. On increasing the

cutting speed, the lines become more continuous, which indicates an increase in the machining process stability.

The use of variable feed per tooth has a minor effect on the milling process dynamics, as evident from the data in Figure 22. For both tools used, minor changes in the distances between the diagonals and their continuity were observed. This indicates a minor change in the signal dynamics. Better repeatability of the diagonal lines is observed when milling with the helix angle 50° tool. Similar conclusions were drawn from the analyses of this signal of the F_x component obtained by multiscale entropy and FFT.

The most pronounced changes in the recurrence plots are observed when analyzing the measurement signals for different depths of cut, for both cutting tools used (Figure 23). For a_p = 0.5 mm, irregularly broken diagonal lines are visible, indicating the presence of a very complex signal with a large number of harmonics. For a_p = 6.0 mm, the diagonals have a more regular shape, resulting from a more stable milling process.

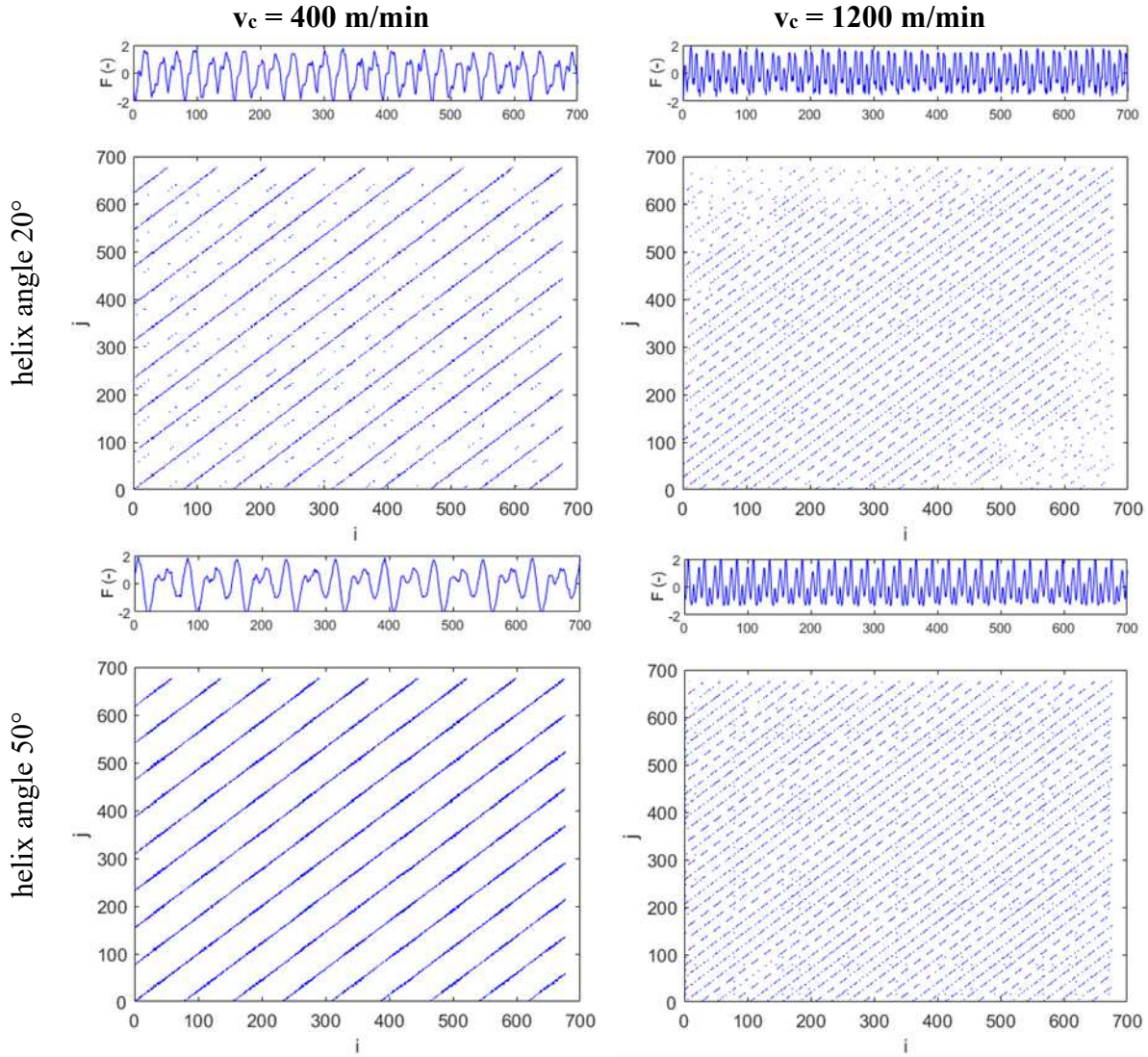


Figure 21. Recurrence plots for cutting force component F_x for different helix angles and variable cutting speed

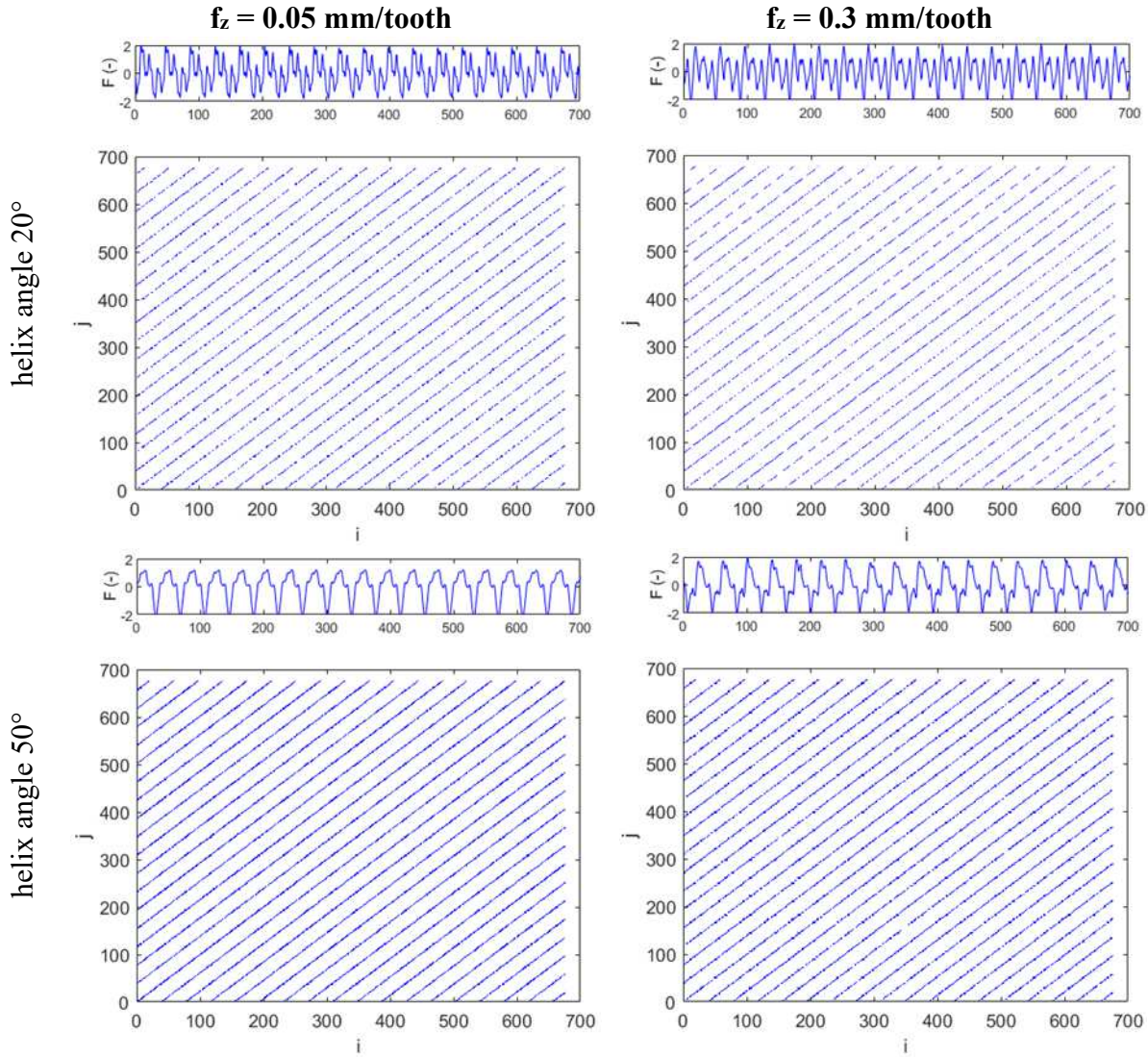
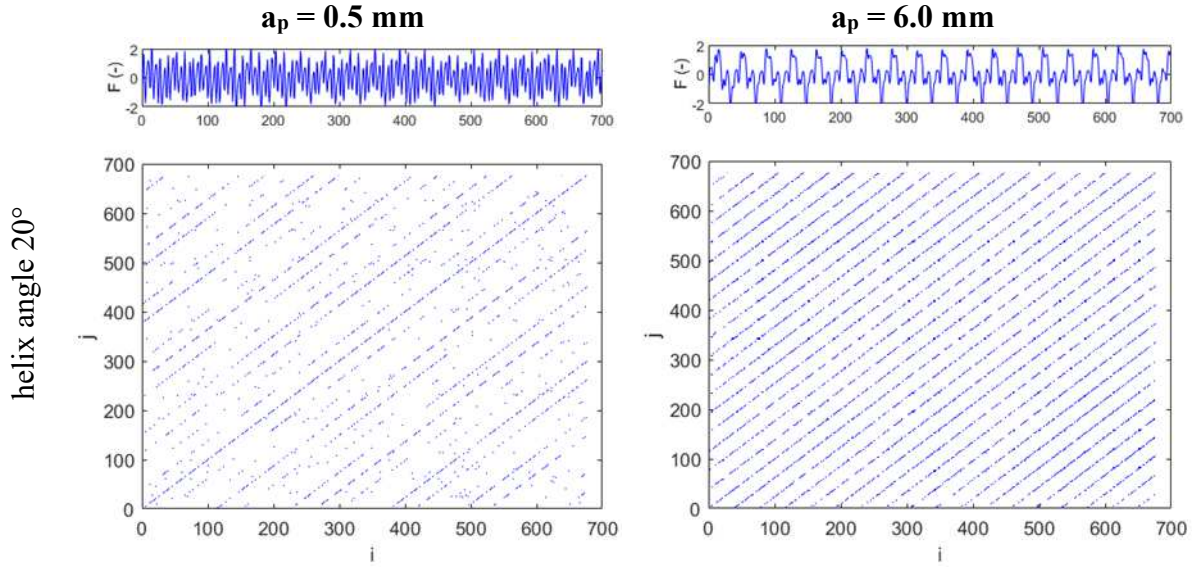


Figure 22. Recurrence plots for cutting force component F_x for different helix angles and variable feed per tooth



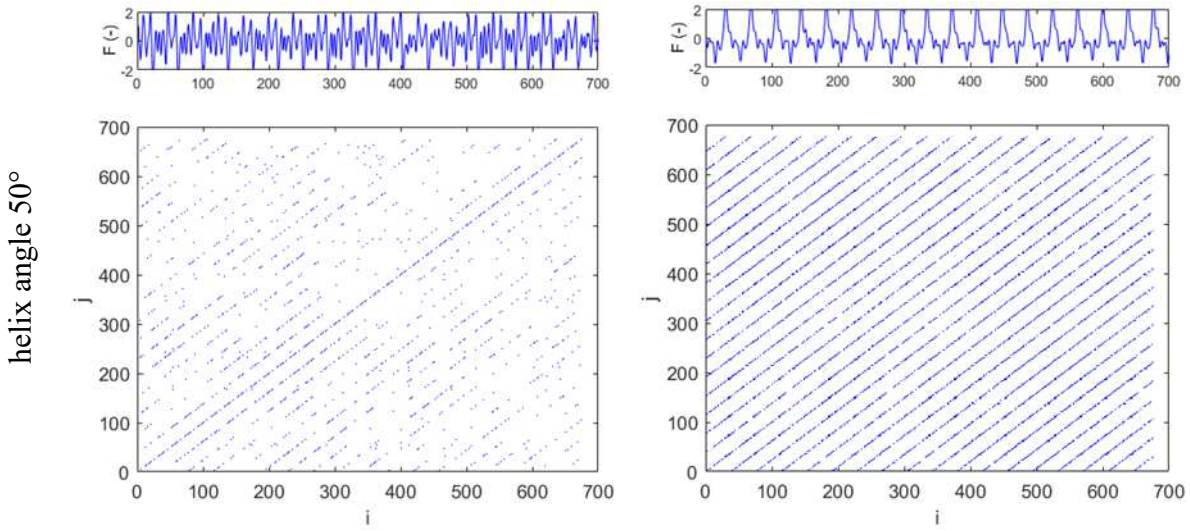


Figure 23. Recurrence plots for cutting force component F_x for different helix angles and variable axial depth of cut

3.5.ANOVA statistical analysis of the cutting force component F_x

Table 3 presents Welch's ANOVA results for the F_x variable as a function of the milling process parameters. The results demonstrate that whatever the helix angle value, a change in feed per tooth exerts a substantial impact on the F_x component of the total cutting force. For both analyzed cases, i.e., $\lambda_s = 20°$ and $\lambda_s = 50°$, the p-value is lower than the significance level $\alpha = 0.05$. Regarding the qualitative variables, i.e., the cutting speed v_c and the depth of cut a_p, their influence on the F_x component is significant in milling with $\lambda_s = 20°$. To identify statistically significant differences between the analyzed groups, a post-hoc Games-Howell test was performed, the findings of which are listed in Table 4. The post-hoc test results (Table 4) show that in milling with $\lambda_s = 20°$, increasing the cutting speed from $v_c = 400$ m/min to $v_c = 600$ m/min and from $v_c = 600$ m/min to $v_c = 800$ m/min has no considerable impact on the value of F_x. For the variable feed per tooth f_z and $\lambda_s = 20°$, there are no statistically significant differences in the F_x component value when the feed per tooth is changed from $f_z = 0.20$ mm/tooth to $f_z = 0.25$ mm/tooth. As for the independent variables, i.e., f_z at $\lambda_s = 50°$ and a_p at $\lambda_s = 20°$, by varying the values of all analyzed machining parameters we exert a significant impact on the F_x component value.

Table. 3. Welch's ANOVA results for F_x versus cutting speed (v_c), depth of cut (a_p) and feed per tooth (f_z), where: df1 - degrees of freedom for the variance between groups, df2 - degrees of freedom for the variance within groups, F – value of the test statistic, p - probability level

F_x for λ_s=20°					
Variable	df1	df2	F Welch	p	conclusion
Cutting speed v_c	4	17.2372	878.4690	$p < 0.0001$	$p<\alpha$
Depth of cut a_p	5	19.3131	20519.5700	$p < 0.0001$	$p<\alpha$
Feed per tooth f_z	5	17.0033	20174.5100	$p < 0.0001$	$p<\alpha$
Fx for λ_s=50°					
Variable	df1	df2	F Welch	p	conclusion
Feed per tooth f_z	5	18.5864	23733.7600	$p < 0.0001$	$p<\alpha$

Table 4. Post-hoc Games-Howell test results for a dependent variable F_x versus cutting speed (v_c), feed per tooth (f_z) and depth of cut (a_p). The level of probability with no statistically significant differences is marked in red

Cutting speed v_c						
	400	600	800	1000	1200	
400		**0.13500**	0.00091	0.00001	0.00000	
600	**0.13500**		**0.94800**	0.00015	0.00000	
800	0.00091	**0.94800**		0.00000	0.00000	
1000	0.00001	0.00015	0.00000		0.00000	
1200	0.00000	0.00000	0.00000	0.00000		
Feed per tooth f_z for λ_s=20°						
	0.05	0.10	0.15	0.20	0.25	0.30
0.05		0.00000	0.00000	0.00000	0.00000	0.00000
0.10	0.00000		0.00000	0.00000	0.00000	0.00000
0.15	0.00000	0.00000		0.00000	0.00000	0.00000
0.20	0.00000	0.00000	0.00000		**0.75900**	0.00900
0.25	0.00000	0.00000	0.00000	**0.75900**		0.04700
0.30	0.00000	0.00000	0.00000	0.00900	0.04700	
Feed per tooth f_z for λ_s=50°						
	0.05	0.10	0.15	0.20	0.25	0.30
0.05		0.00000	0.00000	0.00000	0.00000	0.00000
0.10	0.00000		0.00000	0.00000	0.00000	0.00000
0.15	0.00000	0.00000		0.00000	0.00000	0.00000
0.20	0.00000	0.00000	0.00000		0.00000	0.01200
0.25	0.00000	0.00000	0.00000	0.00000		0.00067
0.30	0.00000	0.00000	0.00000	0.01200	0.00067	
Depth of cut a_p						
	0.5	1.0	1.5	3.0	4.5	6
0.5		0.00000	0.00000	0.00000	0.00000	0.00005
1.0	0.00000		0.00000	0.00000	0.00000	0.00000
1.5	0.00000	0.00000		0.00000	0.00000	0.00000
3.0	0.00000	0.00000	0.00000		0.00000	0.00000
4.5	0.00000	0.00000	0.00000	0.00000		0.00000
6.0	0.00005	0.00000	0.00000	0.00000	0.00000	

Results of the non-parametric Kruskal-Wallis test (Table 5) show that for λ_s = 50°, the cutting force component F_x is strongly affected by the cutting speed v_c and the depth of cut a_p. A multiple comparison of mean ranks (Table 6) for the F_x component obtained with λ_s = 50° reveals that increasing the cutting speed from v_c = 400 m/min to v_c = 800 m/min, as well as from v_c = 800 m/min to vc = 1200 m/min and from v_c = 1000 m/min to v_c = 1200 m/min results in statistically significant differences in the F_x component values. Regarding the dependence between a_p and F_x, increasing the depth of cut from a_p = 0.5 mm to a_p = 3.0 mm, 4.5 mm and 6.0 mm, as well as from a_p = 1.0 mm to a_p = 4.5 mm and 6.0 mm, and from a_p = 1.5 mm to a_p = 6.0 mm induces statistically significant differences in the value of the analyzed dependent variable.

Table 5. Kruskal-Wallis test results for F_x (where: p - probability level)

F_x for λ_s=50°			
Variable			conclusion
Cutting speed v_c	KW H (4;n=40) = 37.46341	0.0000	p<α
Depth of cut a_p	KW H (5;n=48) = 44.51631	0.0000	p<α

Table 6. Multiple comparison of mean ranks for F_x depending on the cutting speed v_c and the depth of cut a_p. The level of probability with no statistically significant differences is marked in red

	Cutting speed v_c				
	400	600	800	1000	1200
400		**1.00000**	0.00040	**0.06195**	**1.00000**
600	**1.00000**		**0.06195**	**1.00000**	**0.06195**
800	0.00040	**0.06195**		**1.00000**	0.00000
1000	**0.06195**	**1.00000**	**1.00000**		0.00040
1200	**1.00000**	**0.06195**	0.00000	0.00040	

	Depth of cut a_p					
	0.5	1.0	1.5	3.0	4.5	6
0.5		**1.00000**	**0.33406**	0.00185	0.00047	0.00000
1.0	**1.00000**		**1.00000**	**0.10513**	0.03818	0.00007
1.5	**0.33406**	**1.00000**		**1.00000**	**0.91189**	0.00910
3.0	0.00185	**0.10513**	**1.00000**		**1.00000**	**0.91189**
4.5	0.00047	0.03818	**0.91189**	**1.00000**		**1.00000**
6.0	0.00000	0.00007	0.00910	**0.91189**	**1.00000**	

4. Discussion

Results reported in this paper complement the research investigating relationships between tool geometry and selected machinability indicators, specifically the cutting force component F_x. A similar study was conducted in 2014 [34] to determine the impact of technological parameters and rake angle on cutting force components and their amplitudes. That study focused, however, only on the AZ91D alloy. The present study undertook to extend the scope of research results to include, among others, box plots, peak-to-peak and root mean square values. Moreover, the current study presents the results of composite multiscale entropy, FFT analysis and recurrence plots. A detailed statistical analysis was made by ANOVA and post-hoc tests. Simple results reported in [34] detected the presence of a characteristic, high-speed machining range. In this region one can usually observe a drop in the components of the total cutting force and the cutting zone temperature. Comparing three levels of variation in v_c and f_z as well as four different axial depths of cut a_p, the following can be established. The highest cutting force components (F_x, F_y, F_z) occurred at the lowest tested cutting speed, i.e., at v_c = 400 m/min. The highest value was obtained when machining was conducted with $\gamma = 5°$, v_c = 400 m/min and F_x = 747 N (in the directions Y and Z, the components had lower values). The use of low and mid feed per tooth values led to an increase in all force components, while at higher feeds -- they became stable. An increase in the feed per tooth value from 0.05 to 0.15 mm/tooth at variable depth of cut led to an increase in all cutting force components.

An analysis of two tested axial depths of cut (for two feeds per tooth) revealed – as expected – a nearly linear increase in the cutting force component values and their amplitudes. The F_x component was below approx. 600 N at f_z = 0.15 mm/tooth and approx. 350 N at f_z = 0.05

mm/tooth. Lower cutting force component values and amplitudes were observed for the tool with a rake angle of $\gamma = 30°$, indicating improved stabilization of the machining process. This effect may be attributed to the more favorable, sharper tool geometry compared to the tool described by $\gamma = 5°$, as well as to potentially reduced deformation in the shear zone. This observation is also important from the perspective of machining safety, since lower cutting forces in the cutting zone may contribute to reduced heat generation and, consequently, lower temperatures. It is therefore of great relevance to magnesium alloys machining, where excessive cutting zone temperature may increase the likelihood of chip ignition.

Similar analyses were conducted in 2022 [40, 52] using, among others, a two-flute carbide cutter with a helix angle of 30°. In [52] the analysis was conducted for the AZ31B wrought alloy, while in [40] for the AZ91D die-casting alloy. The AZ31B alloy's machinability was examined, showing that high-speed milling made the cutting force component values decrease upon entering the high-speed machining range. The F_x component generally achieved the highest values in relation to the parameters under analysis. The study captured 3 components of the total cutting force and analyzed the quantities such as the maximum value (F_{max}), the amplitude of cutting force components (F_{amp}), and the root mean square value (F_{rms}). Moreover, the study offered an analysis by composite multiscale entropy and artificial neural networks simulations. The results demonstrated that for the so-called low ranges of v_c, the cutting force components would increase in all three directions, whereas they would decrease at high values of v_c, which is typical of the region defined as HSM. Irrespective of the technological parameters or tool type, using the investigated parameters, the highest values were usually recorded for the cutting force component F_x, much like in previous studies (for tools with different rake angles). Regardless of the end mill type or technological specifications, an increase in feed per tooth caused a linear rise in the values of all cutting force components. The cutting force component signals recorded at the highest values of the examined technological parameters exhibited a lesser degree of disorder, as shown by the CMSE analysis. A study on the AZ91D alloy [40] subjected to machining using a two-flute carbide cutter with a helix angle of 30° showed that that use of variable parameters had impact on the cutting force components (feed force and normal to the feed component), with the highest values observed for the feed component. Individual cutting force components depended more on feeds rather than on cutting speeds. The cutting force components, as well as their amplitudes and ranges rose approximately linearly and proportionately with an increase in feed per tooth. It is interesting to note that when the cutting speed was increased to 1200 m/min, the total cutting force components dropped. This could be a sign of increased machining stability and entering the high-speed machining range.

An analysis of cutting zone temperature is as important as that of cutting forces. The cutting force components can have a direct impact on the temperature at tool-workpiece contact. Given the decohesion mechanism, this impact may also extend to the chip temperature that is induced during machining. For the analyzed cutting tools, the chip temperature [9] was below approx. 420 °C. This value can be considered relatively safe in dry rough milling. A detailed analysis of magnesium alloy machinability, taking into account the temperature of chips, led to the following observations. Higher cutting speeds could be used in the dry rough milling of magnesium alloys without chip ignition danger (no typical mode of chip ignition was observed). In terms of individual technological parameters under analysis, the maximum chip temperature did not exceed the following values: 362.95 °C for cutting speed, 417.74 °C for feed per tooth, and 358.13 °C for axial depth of cut. These are important findings in the context of safety during dry milling of magnesium alloys.

5. Conclusions

When designing a machining process, technological parameters must be carefully selected to ensure the optimum and most stable results. Among the key elements affecting process stability are the machining parameters and the rigidity of machine tools. In this study, different helix angles and values of the technological parameters were tested to assess the cutting force components and their amplitudes during AZ91D magnesium alloy machining. The findings of the study lead to the following conclusions:

- For a variety of machining conditions, the rough milling process could be carried out effectively without a considerable increase in the normal to the feed force component.
- When altering the technological milling parameters, notable differences were observed depending on the tool shape (helix angle); these variations occurred under all machining conditions.
- Box plot analyses revealed that the ranges of the studied parameters would increase with the cross-section of the cut layer (i.e., feed per tooth and depth of cut); additionally, the presence of regions "free" from extreme or outlier data was identified.
- In terms of cutting tool geometry, considerably fewer regions with extreme values or outliers were observed for the tool with a helix angle of 20° compared to the 50° helix angle tool.
- An analysis of the cutting speed and box plots revealed that the optimum conditions in terms of the normal to the feed force component range and lack of outliers / extreme values occurred at v_c 400 m/min and in the range 1000-1200 m/min (for the 20° tool, no outliers / extreme values were observed for the entire tested cutting speed range).
- The smallest scatter of the cutting speed results was observed at v_c = 1200 m/min, indicating entry into the high-speed machining range, which is a positive effect of using high cutting speeds for enhancing process efficiency.
- An analysis of the maximum, peak-to-peak and root mean square values showed that they were the highest for the mid tested cutting speed value of v_c = 800 m/min and for the 50° tool, amounting to $F_{x\text{-}max} \approx$ 767 N, $F_{peak\text{-}to\text{-}peak} \approx$ 1493 N, $F_{RMS} \approx$ 359–376 N (for 800 and 1000 m/min), respectively.
- An analysis of feeds per tooth and box plots showed that the optimum machining conditions, without regions having outliers / extreme values, occurred at low and very high feeds per tooth (0.05 and 0.30 mm/tooth); also, for the 20° tool, no outliers / extreme values occurred in the entire tested feed per tooth range.
- The smallest scatter of feed per tooth results occurred within the range between 0.05 and 0.10 mm/tooth; any further increase in the feed per tooth value, and hence in the cross-section of the cut layer caused a greater scatter between the results. For the feed per tooth ranging 0.20–0.30 mm/tooth, the normal to the feed force component value became stable.
- An analysis of the remaining results ($F_{x\text{-}max}$, $F_{peak\text{-}to\text{-}peak}$, F_{RMS}) made it possible to conclude that they were the highest and similar for the feed range 0.20–0.30 mm/tooth, their values being as follows: $F_{x\text{-}max} \approx$ 635–651 N, $F_{peak\text{-}to\text{-}peak} \approx$ 1172–1204 N, $F_{RMS} \approx$ 254–258 N (for the 20° tool); and $F_{x\text{-}max} \approx$ 834–886 N, $F_{peak\text{-}to\text{-}peak} \approx$ 1655–1696 N, $F_{RMS} \approx$ 369–425 N (for the 50° tool).
- An analysis of axial depths of cut and box plots revealed that the optimum machining conditions occurred at a_p = 0.5 to 3.0 mm, whereas for other cases there was a clear increase in the presence of outliers or extreme values.

- Other results for axial depth of cut did not exceed the following values: $F_{x\text{-}max} \approx 736$ N, $F_{peak\text{-}to\text{-}peak} \approx 1311$ N, $F_{RMS} \approx 259$ N, these were the highest values for the largest cross-section of the cut layer and hence for the highest values of a_p.
- For the majority of cases, the maximum, peak-to-peak and root mean square values were lower for the 20° tool, so this tool is recommended for dry roughing of magnesium alloys.
- Significantly lower entropy values were observed in milling with the 50° tool for all analyzed cutting speeds. The use of this tool is advantageous due to the lower complexity of the milling process dynamics.
- An increase in feed per tooth caused a proportional increase in the entropy value calculated for both tools. However, lower entropy values were observed in milling with the 50° tool.
- Regarding the effect of axial depth of cut, similar entropy values were obtained for both tools. The entropy value dropped sharply with increasing the axial depth of cut.
- The FFT analysis of the signal demonstrated that an increase in cutting speed would reduce the number of harmonics while simultaneously decreasing their amplitudes. This effect was visible for both tools used. This is a beneficial phenomenon, as a lower number of harmonics significantly reduces the likelihood of undesirable self-excited vibrations during machining.
- An increase in feed per tooth caused a gradual decrease in the number of harmonics in the analyzed signal spectrum. Fewer harmonics, especially in the higher frequency range, were observed in milling with the 50° tool.
- Varying the axial depth of cut had the greatest influence on the signal spectrum. As this depth of cut was increased, a sharp decrease in the number of harmonics was observed. This effect was particularly noticeable at higher frequencies and with the 50° tool.
- An analysis of the extreme cutting speed values via recurrence plots showed that at $v_c = 1200$ m/min, the diagonal lines of the plots became more continuous. This indicates increased stability of the machining process.
- The dynamics of the milling process was little affected by varying feed per tooth. For both tools used, minor changes in the distance between the diagonals and their continuity were observed. Better repeatability of the diagonal lines was observed when the milling operation was performed with the 50° helix angle tool. Similar conclusions were drawn from the analyses by multiscale entropy and FFT.
- The greatest impact on the behavior pattern of recurrence plots was exerted by increasing the axial depth of cut from $a_p = 0.5$ mm to $a_p = 6.0$ mm. For both tools used, the diagonal lines in the recurrence plots were observed at $a_p = 6.0$ mm, which was due to a higher stability of the milling process.
- Summarizing the presented findings, it can be concluded that using a tool with a 20° angle during milling limits the force level and the number of extreme values, whereas milling with a 50° tool results in more regular signal dynamics.

Acknowledgments / Funding
This research was supported by FD-20/IM-5/138, FD-20/IM-5/131, FD-20/IM-5/061 and FD-20/IM-5/107.

A conflict of interest
On behalf of all authors, the corresponding author states that there is no conflict of interest.

Data availability

The raw/processed data required to reproduce these findings cannot be shared at this time as the data also forms part of an ongoing study.

References

1. Čuš F, Župerl U, Gečevska V (2007) High-speed milling of light metals. Journal of achievements in materials and manufacturing engineering

2. Zawada-Michałowska M, Józwik J, Legutko S, et al (2020) Cutting Force during Surface Layer Milling of Selected Aluminium Alloys. Materials 13:5725. https://doi.org/10.3390/MA13245725

3. Danis I, Monies F, Lagarrigue P, Wojtowicz N (2016) Cutting forces and their modelling in plunge milling of magnesium-rare earth alloys. International Journal of Advanced Manufacturing Technology 84:1801–1820. https://doi.org/10.1007/S00170-015-7826-3/METRICS

4. Zagórski I, Kuczmaszewski J (2018) Temperature measurements in the cutting zone, mass, chip fragmentation and analysis of chip metallography images during AZ31 and AZ91HP magnesium alloy milling. Aircraft Engineering and Aerospace Technology 90:496–505. https://doi.org/10.1108/AEAT-12-2015-0254

5. Zgórniak P, Stachurski W, Ostrowski D (2016) Application of thermographic measurements for the determination of the impact of selected cutting parameters on the temperature in the workpiece during milling process. Strojniski Vestnik/Journal of Mechanical Engineering 62:657–664. https://doi.org/10.5545/SV-JME.2015.3259

6. Bhagat KC, Kumar A, Thakur A, Gangopadhyay S (2024) Analysis of cutting forces and surface quality during micro milling of AZ31B magnesium alloy. International Journal of Advanced Manufacturing Technology 134:3465–3480. https://doi.org/10.1007/S00170-024-14315-Y/FIGURES/15

7. Bhagat KC, Thakur A, Gangopadhyay S (2026) Effect of Cutting Parameters Using Uncoated and Coated Carbide Tools on Cutting Force During Micro-Milling of AZ31B Magnesium Alloy. Lecture Notes in Mechanical Engineering 19–33. https://doi.org/10.1007/978-981-96-5550-2_3

8. Shi K, Zhang D, Ren J, et al (2016) Effect of cutting parameters on machinability characteristics in milling of magnesium alloy with carbide tool. Advances in Mechanical Engineering 8:. https://doi.org/10.1177/1687814016628392/ASSET/47BB6E2E-5B04-465B-85F3-CD9CC34A5C42/ASSETS/IMAGES/LARGE/10.1177_1687814016628392-FIG8.JPG

9. Zagórski I, Zgórniak P, Habrat W, et al (2024) Methodology of Chip Temperature Measurement and Safety Machining Assessment in Dry Rough Milling of Magnesium Alloys Using Different Helix Angle Tools. Materials 17:2063. https://doi.org/10.3390/MA17092063

10. Bolar G, Adhikari R, Nayak SN, Joshi SN (2022) Assessment of ignition risk in dry helical hole milling of AZ31 magnesium alloy considering the machining temperature and chip morphology. J Manuf Process 77:260–271. https://doi.org/10.1016/J.JMAPRO.2022.03.023

11. Kuczmaszewski J, Zagórski I, Gziut O, et al (2017) Chip fragmentation in the milling of AZ91HP magnesium alloy. Strojniski Vestnik/Journal of Mechanical Engineering 63:628–642. https://doi.org/10.5545/SV-JME.2017.4406

12. Weremczuk A, Kęcik K, Rusinek R, Warmiński J (2013) The dynamics of the cutting process with Duffing nonlinearity. Eksploatacja i Niezawodność Vol. 15:209–213

13. Sivam SSSP, Bhat MDJ, Natarajan S, Chauhan N (2018) ANALYSIS OF RESIDUAL STRESSES, THERMAL STRESSES, CUTTING FORCES AND OTHER OUTPUT RESPONSES OF FACE MILLING OPERATION ON ZE41 MAGNESIUM ALLOY. International Journal of Modern Manufacturing Technologies 2067–3604

14. Buldum BB, Leksycki K, Cagan SC (2025) Comparative Analysis of Dry, Minimum Quantity Lubrication, and Nano-Reinforced Minimum Quantity Lubrication Environments on the Machining Performance of AZ91D Magnesium Alloy. Machines 13:430. https://doi.org/10.3390/MACHINES13050430

15. Alshibi A, Nasreldin A, Pervaiz S (2023) Sustainable Vegetable Oil-Based Minimum Quantity Lubrication Assisted Machining of AZ91 Magnesium Alloy: A Grey Relational Analysis-Based Study. Lubricants 11:. https://doi.org/10.3390/LUBRICANTS11020079

16. Shah R, Shirvani KA, Przyborowski A, et al (2022) Role of Nanofluid Minimum Quantity Lubrication (NMQL) in Machining Application. Lubricants 10:266. https://doi.org/10.3390/LUBRICANTS10100266

17. Xu J, Shen J, Li L, et al (2023) Milling machinability analysis of GW63K rare-earth magnesium alloys based on the concept of clean cutting. Journal of Materials Research and Technology 26:9380–9391. https://doi.org/10.1016/J.JMRT.2023.09.209

18. Li L, Xu J, Guo G, et al (2023) Wear behavior of different coated tools in MQL-assisted milling of magnesium-based rare-earth alloys. Journal of Materials Research and Technology 27:1665–1682. https://doi.org/10.1016/J.JMRT.2023.10.003

19. Saravanan R, Sathish T, Vijayan V, et al (2023) Eco-friendly MoS2/waste coconut oil nanofluid for machining of magnesium implants. Reviews on Advanced Materials Science 62:. https://doi.org/10.1515/RAMS-2022-0296

20. Kumar A, Sharma L, Gill SS (2025) Experimental study on sustainable machining of magnesium-based AZ91D alloy under various cutting parameters. Surface Review and Letters. https://doi.org/10.1142/S0218625X25501434

21. Atasoy Ş, Kandemir S (2024) Machinability investigation on CNC milling of recycled short carbon fiber reinforced magnesium matrix composites. Mater Res Express 11:126501. https://doi.org/10.1088/2053-1591/AD966B

22. Akgün M (2023) Measurement and optimization of cutting forces, surface roughness and temperature in turning of AZ91 Mg alloy. Sadhana - Academy Proceedings in Engineering Sciences 48:60-. https://doi.org/10.1007/S12046-023-02113-3/TABLES/14

23. Adhikari R, Bolar G, Shanmugam R, Koklu U (2023) Machinability and surface integrity investigation during helical hole milling in AZ31 magnesium alloy. International Journal of Lightweight Materials and Manufacture 6:149–164. https://doi.org/10.1016/J.IJLMM.2022.09.006

24. Pleta A, Niaki FA, Mears L (2018) A comparative study on the cutting force coefficient identification between trochoidal and slot milling. Procedia Manuf 26:570–579. https://doi.org/10.1016/J.PROMFG.2018.07.067

25. Pleta A, Niaki FA, Mears L (2017) Investigation of Chip Thickness and Force Modelling of Trochoidal Milling. Procedia Manuf 10:612–621. https://doi.org/10.1016/J.PROMFG.2017.07.063

26. Fu Z, Yang W, Wang X, Leopold J (2015) Analytical Modelling of Milling Forces for Helical End Milling Based on a Predictive Machining Theory. Procedia CIRP 31:258–263. https://doi.org/10.1016/J.PROCIR.2015.03.013

27. Monies F, Danis I, Bes C, et al (2017) A new machining strategy for roughing deep pockets of magnesium-rare earth alloys. International Journal of Advanced Manufacturing Technology 92:3883–3901. https://doi.org/10.1007/S00170-017-0444-5/METRICS

28. Monies F, Danis I, Lagarrigue P, et al (2017) Balancing of the transversal cutting force for pocket milling cutters: application for roughing a magnesium-rare earth alloy. International Journal of Advanced Manufacturing Technology 89:45–64. https://doi.org/10.1007/S00170-016-9011-8/METRICS

29. Erçetin A, Aslantas K, Özgün Ö (2020) Micro-end milling of biomedical Tz54 magnesium alloy produced through powder metallurgy. Machining Science and Technology 24:924–947. https://doi.org/10.1080/10910344.2020.1771572

30. Wu X, Liu L, Du M, et al (2020) Experimental Study on the Minimum Undeformed Chip Thickness Based on Effective Rake Angle in Micro Milling. Micromachines (Basel) 11:924. https://doi.org/10.3390/MI11100924

31. Salguero J, Batista M, Calamaz M, et al (2013) Cutting Forces Parametric Model for the Dry High Speed Contour Milling of Aerospace Aluminium Alloys. Procedia Eng 63:735–742. https://doi.org/10.1016/J.PROENG.2013.08.215

32. Kecik K, Borowiec M, Rusinek R (2016) Verification of the stability lobes of Inconel 718 milling by recurrence plot applications and composite multiscale entropy analysis. The European Physical Journal Plus 2016 131:1 131:14-. https://doi.org/10.1140/EPJP/I2016-16014-X

33. Görög A, Stančeková D, Kapustová M, et al (2017) Influence of selected cutting conditions on cutting forces. Advances in Science and Technology Research Journal 11:179–185. https://doi.org/10.12913/22998624/66508

34. Gziut O, Kuczmaszewski J, Zagórski I (2014) The Influence of Technological Parameters and Geometric Features of a Cutting Edge on Cutting Forces during AZ91HP Alloy Milling. Advances in Manufacturing Science and Technology 38:83–92. https://doi.org/10.2478/AMST-2014-0013

35. Plodzien M, Burek J, Zylka L, Sulkowicz P (2020) The influence of end mill helix angle on high performance milling process. Journal of Mechanical Science and Technology 34:817–827. https://doi.org/10.1007/S12206-020-0131-6/METRICS

36. Aydın M, Köklü U (2024) Analysis of cutting forces at different spindle speeds with straight and helical-flute tools for conventional-speed milling incorporating the effect of

tool runout. Mechanics Based Design of Structures and Machines 52:867–893. https://doi.org/10.1080/15397734.2022.2125878

37. Biruk-Urban K, Józwik J, Bere P (2022) Cutting Forces and 3D Surface Analysis of CFRP Milling. Advances in Science and Technology Research Journal 16:206–215. https://doi.org/10.12913/22998624/147338

38. Bayraktar S, Turgut Y (2016) Investigation of the cutting forces and surface roughness in milling carbon-fiber-reinforced polymer composite material. Materiali in tehnologije / Materials and technology 50:591–600. https://doi.org/10.17222/mit.2015.199

39. Kuczmaszewski J, Pieśko P (2014) Wear of milling cutters resulting from high silicon aluminium alloy cast AlSi21CuNi machining. Eksploatacja i Niezawodność 16:

40. Zagorski I (2022) Cutting force components in rough milling of magnesium alloys with a TiAlN-coated carbide tool. 2022 IEEE 9th International Workshop on Metrology for AeroSpace, MetroAeroSpace 2022 - Proceedings 64–69. https://doi.org/10.1109/METROAEROSPACE54187.2022.9856171

41. Weremczuk A, Rusinek R, Warminski J (2015) The Concept of Active Elimination of Vibrations in Milling Process. Procedia CIRP 31:82–87. https://doi.org/10.1016/J.PROCIR.2015.03.036

42. Weremczuk A, Rusinek R, Warminski J (2018) Bifurcation and stability analysis of a nonlinear milling process. AIP Conf Proc 1922:. https://doi.org/10.1063/1.5019093/608609

43. Litak G, Syta A, Rusinek R (2011) Dynamical changes during composite milling: Recurrence and multiscale entropy analysis. International Journal of Advanced Manufacturing Technology 56:445–453. https://doi.org/10.1007/S00170-011-3195-8/METRICS

44. Altintas Y, Stepan G, Merdol D, Dombovari Z (2008) Chatter stability of milling in frequency and discrete time domain. CIRP J Manuf Sci Technol 1:35–44. https://doi.org/10.1016/J.CIRPJ.2008.06.003

45. Marwan N, Romano MC, Thiel M, Kurths J (2007) Recurrence plots for the analysis of complex systems. Phys Rep 438:237–329. https://doi.org/10.1016/j.physrep.2006.11.001

46. Ciecieląg K (2024) Influence of the Cooling Method on Cutting Force and Recurrence Analysis in Polymer Composite Milling. Materials 17:5981. https://doi.org/10.3390/MA17235981

47. Kecik K, Ciecieląg K (2025) The effect of cutting parameters on defect detection based on recurrence analysis of cutting force signals obtained from GFRP composite milling. Measurement 239:115406. https://doi.org/10.1016/J.MEASUREMENT.2024.115406

48. Weremczuk A, Borowiec M, Rudzik M, Rusinek R (2018) Stable and unstable milling process for nickel superalloy as observed by recurrence plots and multiscale entropy. Eksploatacja i Niezawodność – Maintenance and Reliability 20:318–326. https://doi.org/10.17531/EIN.2018.2.19

49. Wu S De, Wu CW, Lin SG, et al (2013) Time Series Analysis Using Composite Multiscale Entropy. Entropy 15:1069–1084. https://doi.org/10.3390/E15031069

50. Litak G, Kecik K, Rusinek R (2013) Cutting force response in milling of Inconel: analysis by wavelet and Hilbert-Huang Transforms. Latin American Journal of Solids and Structures 10:133–140. https://doi.org/10.1590/S1679-78252013000100013

51. Ciecieląg K, Kecik K, Zaleski K (2020) Defects detection from time series of cutting force in composite milling process by recurrence analysis. Journal of Reinforced Plastics and Composites 39:890–901. https://doi.org/10.1177/0731684420935985

52. Kulisz M, Zagórski I, Weremczuk A, et al (2022) Analysis and prediction of the impact of technological parameters on cutting force components in rough milling of AZ31 magnesium alloy. Archives of Civil and Mechanical Engineering 22:. https://doi.org/10.1007/s43452-021-00319-y

53. Suneesh E, Sivapragash M (2021) Multi-response optimisation of micro-milling performance while machining a novel magnesium alloy and its alumina composites. Measurement 168:108345. https://doi.org/10.1016/J.MEASUREMENT.2020.108345

54. Biruk-Urban K, Bere P, Józwik J, Leleń M (2022) Experimental Study and Artificial Neural Network Simulation of Cutting Forces and Delamination Analysis in GFRP Drilling. Materials 15:8597. https://doi.org/10.3390/MA15238597

55. Darshan S, Desai KA, Bhattacharyya A (2025) Physics-informed experimental design for neural network-based cutting force model in end milling of carbon fiber reinforced polymer composites. J Manuf Process 142:440–452. https://doi.org/10.1016/J.JMAPRO.2025.03.100

56. Zagórski I, Weremczuk A, Kulisz M, Skoczylas A (2025) Vibration and stability in dry rough milling AZ31B magnesium alloy using end mills with different edge geometry. Measurement 256:118523. https://doi.org/10.1016/J.MEASUREMENT.2025.118523